October 2, 1974

AMERICAN
INSTITUTE OF
AERONAUTICS AND
ASTRONAUTICS

1290 AVENUE
OF THE AMERICAS
NEW YORK, N.Y. 10019
TELEPHONE
212/581-4300

To: Gifford A. Young

From: Ruth F. Bryans, Director, Scientific Publications

A back-up paper is enclosed for the following Synoptic:

Author(s): Dara W. Childs

Title of Synoptic: Transient Rotordynamic Analysis for the Space-Shuttle Main Engine High-Pressure Oxygen Turbopump (Log No. A5146)

Title of Back-up Paper: same

Correspondence with:

Associate Professor Dara W. Childs
Department of Mechanical Engineering
Speed Scientific School
James Breckenridge Speed Foundation
University of Louisville
Louisville, Kentucky 40208

Journal: Journal of Spacecraft and Rockets

Scheduled Issue: February 1975

Ruth F. Bryans

(Miss) Ruth F. Bryans

RFB:jg
Enc.

(NASA-CR-140455) TRANSIENT ROTORDYNAMIC ANALYSIS FOR THE SPACE-SHUTTLE MAIN ENGINE HIGH-PRESSURE OXYGEN TURBOPUMP (Louisville Univ.) 49 p HC $5.50 CSCL 13I G3/15

N74-34003

Unclas
50666

ALLEN E. PUCKETT, President, DAVID C. HAZEN, Vice President-Education, GORDON L. DUGGER, Vice President-Publications, FREDERICK L. BAGBY, Vice President-Section Affairs, HOLT ASHLEY, Vice President-Technical, ROBERT W. RUMMEL, Treasurer, ALLAN D. EMIL, Legal Counsel

STAFF OFFICERS: JAMES J. HARFORD, Executive Secretary, ROBERT R. DEXTER, Secretary, JOSEPH J. MAITAN, Controller

DIRECTORS: MAC C. ADAMS, J. EDWARD ANDERSON, ROBERT C. COLLINS, HARVEY M. COOK, A. SCOTT CROSSFIELD, CHARLES W. DUFFY, JR., HERBERT FOX, JOSEPH G. GAVIN, JR., MARTIN GOLAND, ROBERT E. HAGE, GRANT L. HANSEN, EDWARD H. HEINEMANN, CHRISTOPHER C. KRAFT, JR., PAUL A. LIBBY, EUGENE S. LOVE, WALTER T. OLSON, MAYNARD L. PENNELL, ALAN Y. POPE, CARLOS C. WOOD

TRANSIENT ROTORDYNAMIC ANALYSIS FOR THE SPACE-SHUTTLE MAIN ENGINE HIGH-PRESSURE OXYGEN TURBOPUMP

By

Dara W. Childs

February 8, 1974

Backup Document for AIAA Synoptic Scheduled for Publication in the Journal of Spacecraft and Rockets, February 1975

Department of Mechanical Engineering
Speed Scientific School
James Breckenridge Speed Foundation
University of Louisville
Louisville, Kentucky 40208

SYNOPTIC BACKUP DOCUMENT

This document is made publicly available through the NASA scientific and technical information system as a service to readers of the corresponding "Synoptic" which is scheduled for publication in the following (checked) technical journal of the American Institute of Aeronautics and Astronautics.

- [ ] AIAA Journal
- [ ] Journal of Aircraft
- [X] Journal of Spacecraft & Rockets, February 1975
- [ ] Journal of Hydronautics

A Synoptic is a brief journal article that presents the key results of an investigation in text, tabular, and graphical form. It is neither a long abstract nor a condensation of a full length paper, but is written by the authors with the specific purpose of presenting essential information in an easily assimilated manner. It is editorially and technically reviewed for publication just as is any manuscript submission. The author must, however, also submit a full backup paper to aid the editors and reviewers in their evaluation of the synoptic. The backup paper, which may be an original manuscript or a research report, is not required to conform to AIAA manuscript rules.

For the benefit of readers of the Synoptic who may wish to refer to this backup document, it is made available in this microfiche (or facsimile) form without editorial or makeup changes.

TRANSIENT ROTORDYNAMIC ANALYSIS FOR THE SPACE-SHUTTLE MAIN ENGINE HIGH-PRESSURE OXYGEN TURBOPUMP*

DARA W. CHILDS**
THE UNIVERSITY OF LOUISVILLE
LOUISVILLE, KY.

A simulation study has been conducted to examine the transient rotordynamics of the space shuttle main engine (SSME) high pressure oxygen turbopump (HPOTP) with the objective of identifying, anticipating, and (hopefully) avoiding rotordynamic problem areas. Simulations were performed for steady-state operations at emergency power levels and for critical speed transitions. No problems are indicated in steady-state operation of the HPOTP at emergency power levels. However, the results indicate that a rubbing condition will be experienced during critical speed transition at shutdown. Specifically, for the presently projected rotor deceleration rate and imbalance distribution, rubbing at the turbine floating-ring seals is predicted. This condition can be corrected to some extent by either reducing the imbalance at the HPOTP hot-gas turbine wheels, or by a more rapid deceleration of the rotor through its critical speed.

This study was the result of a cooperative effort by the author, NASA, and Rocketdyne Division of Rockwell International personnel. The rubbing condition indicated for the HPOTP is presently under investigation by both NASA and Rocketdyne personnel. The HPOTP test program has been designed to determine whether or not this rubbing condition will arise, and whether such rubbing

will compromise the operational performance of the HPOTP. Specifically, the test and development program will ascertain the operational integrity of the floating-ring seal.

This study demonstrates the utility of a transient flexible-rotor simulation model as a tool in the development of high-speed flexible rotating equipment. Futhermore, the availability of the model developed in this study will provide a significant analytical reserve for dealing with problems which the SSME may see fit to provide once the test program is underway. For example, the model would be well suited for the examination of alternative hardware "fixes" if an unanticipated unstable whirling mode should appear during the development program.

*This work was performed while the author was a fellow in the 1973 NASA-ASEE summer faculty fellowship program at Marshal Space Flight Center. The NASA counter part for this study was Mr. Loren Gross.

**Associate Professor of Mechanical Engineering and Engineering Management.

INTRODUCTION

A series arrangement of a low-pressure turbopump followed by a high-pressure turbopump is employed on both the lox and fuel flow paths of the SSME (space shuttle main engine). This paper summarizes the significant results of a simulation study (1)* of the transient dynamics of the SSME (space shuttle main engine) high pressure oxygen (HPOTP) and fuel (HPFTP) turbopumps, which had the primary objective of identifying, anticipating and (hopefully) avoiding rotordynamic problems areas. The simulation study (1) consists of a parallel investigation of both the HPOTP and the HPFTP. However, since no problems were revealed for the HPFTP, and a potentially serious operational problem is predicted for the HPOTP, this paper is restricted to the pertinent results for the HPOTP.

The simulation model used in this study was developed by D. Childs (2) to predict the transient motion of flexible rotating equipment. An outline of the structure of this model is provided in Appendix A. The model's transient output includes bearing displacements and reactions, rotor whirl velocity, rotor spin velocity and acceleration, and rotor displacements at selected locations along the shaft. Of these variables, bearing reactions and rotor displacement are the most significant in anticipating problems which may arise during the operation of the turbopumps. Excessive bearing loads result in shortened bearing lifetimes, and excessive deflections cause seal failures, and can potentially lead to catastrophic failure modes.

---

*Denotes listing in reference section.

The SSME turbopumps are presently under development by Rocketdyne Division of Rockwell International, Canoga Park, California. The basic design of the engines is fixed with the development of detailed drawings in progress; however, component testing of turbopump hardware will not begin until approximately June 1974. Rocketdyne's analysis which is pertinent to a rotordynamic investigation is largely complete, and the steps involved in this analysis, together with the requisite results, are listed below:

a. Structural dynamic analysis of the SSME rotating assemblies. This analysis yields a structural dynamic model for the rotating assembly, which is customarily used to calculate rotor critical speed locations and whirling modes. As an aid to the present investigation, Rocketdyne personnel also calculated unsupported or "free-free" natural frequencies and bending modes for the rotor.

b. Calculation of load-deflection properties for the SSME ball bearings. A computer program which is based on the analyses of A. B. Jones (3), (4) is used to calculate the radial stiffness of ball bearings as a function of the axial and radial load carried by the bearing and the running speed of the shaft.

c. The magnitude of the hydrodynamic side loads which act on the turbopump rotating assembly have been estimated.

d. The magnitude and axial distribution of rotor imbalance have been estimated. These estimates are based on both the planned balance procedure and past experiences with similar turbopumps.

The data cited are sufficient to define a transient rotordynamic model. The assistance of Rocketdyne personnel in providing this information is greatly appreciated. In particular, the efforts of Mr. Bernie Rowan, Mr. Miles Butner, and Mr. Bill Brooks have been of considerable value.

Operational testing of the SSME turbopumps will begin in October 1974. The instrumentation which is planned for the test phase will include measurements of transient radial motion of the rotating assembly at five axial locations. The simulation study (1) provides the transient motion for both turbopumps at these locations, and should assist in the understanding of the transient motion data when it becomes available. Conversely, the availability of high-quality data (i.e., calibrated, high-resolution, transient data taken along the length of the rotating assembly) will provide a unique opportunity to remove many of the uncertainties associated with transient rotordynamic modeling. In particular, this data, in conjunction with the present simulation models, will enable a much better indentification of the damping provided by ball bearings, transient and steady-state hydrodynamic forces, rotor imbalance distribution, etc.

The availability of the two models developed in (1) will provide a significant analytical reserve for dealing with problems which the SSME turbopumps may see fit to provide once the test program is underway. For example, the models would

be well suited for the examination of alternative hardware "fixes" if an unanticipated unstable whirling mode should appear during the development program.

SPACE SHUTTLE MAIN ENGINE HIGH PRESSURE OXYGEN TURBOPUMP

General Information

The SSME HPOTP rotating assembly is illustrated in figure 1. At normal power levels, the main stage of this turbopump is to be supplied lox by a low pressure turbopump at a flowrate of approximately 1047 lb./sec. at a pressure of approximately 360 psia. The discharge pressure of this stage is to be approximately 4635 psia, and the bulk of the discharge flow goes directly to the thrust chamber; however, approximately 100 lb./sec. is diverted to the boost stage with an inlet pressure of approximately 4390 psia. The discharge flowrate from the boost stage (7680 psia) feeds the preburners which drive the hot gas turbines for both high-pressure turbopumps. The gas flowrate which drives the turbine approaches it from the rear, i.e., it moves axially towards the pump stages. The turbine develops approximately 22,900 horsepower at the nominal running speed of 29,250 rpm. Turbine torque at these conditions is 4060 ft. lbs. Discharge flowrate from the turbine goes directly to the main thrust chamber. At emergency power levels, the turbopump running speed is increased to 31, 160 rpm, while at minimum power level, the speed is reduced to 20,890 rpm.

Rocketdyne analysis (5) indicates that a hydrodynamic sideload is developed on the rotating assembly of this turbopump due to circumferential pressure variations on both the main and boost stages. These pressure variations are the result of single-discharge designs for both stages, and are assumed here to be proportional

to $\dot{\phi}^2$ (spin-velocity squared). They are modeled by

$$f(\text{boost}) = k_1 \dot{\phi}^2, \quad k_1 = 1.80 \times 10^{-5} \text{ lb. sec.}^2$$
$$f(\text{main}) = k_2 \dot{\phi}^2, \quad k_2 = 1.53 \times 10^{-4} \text{ lb. sec.}^2 \qquad (1)$$

Hence, at emergency power levels, $\dot{\phi}$ = 31,160 rpm (2990 rad./sec.) the side loads for the boost and main stages are 161 and 1370 lbs., respectively. The direction of the loads is fixed relative to the turbopump housing. The two loads are oppositely directed.

The bearings in the HPOTP are designed to react radial loads only. A balance-piston arrangement is provided at the discharge of the mainstage to react axial thrust loadings. The ball bearing used for the forward-duplex-bearing set of the HPOTP is the same as that used for both bearing sets in the HPFTP. The forward and rear bearings preload for the HPOTP are 350 and 550 lbs., respectively. This preload is maintained by loading the outboard and inboard bearings against one another via a Belleville spring.

As would be expected, the radial load-deflection characteristics of a ball bearing depends on both the axial and radial load carried across the bearing and the bearing's speed of rotation. For the magnitude of radial bearing loads developed in this turbopump, the relationship between radial loads and deflections is linear, and is appropriately modeled by a bearing stiffness coefficient. The dependence of this bearing stiffness coefficient on running speed and axial preload is illustrated in figures 2 and 3. The data of figure 2 are for the rear bearings of the HPOTP, while the data for figure 3 are for both the forward bearings of the HPOTP and

both HPFTP bearings. These data were generated by Mr. M. F. Butner, Rocketdyne Division of Rockwell International, Canoga Park, California, via a computerized version of A. B. Jones analyses (3), (4). Since a constant axial preload is a design objective in the bearings, radial stiffness is only dependent on shaft spin speed. For the data presented, the following representation is employed

$$k_f(\text{forward}) = a_{f0} + a_{f1}\dot{\phi} + a_{f2}\dot{\phi}^2 + a_{f3}\dot{\phi}^3 \qquad (2)$$

$a_{f0} = 1.799 \times 10^6$ lb./in.

$a_{f1} = 105.2$ lb. sec. /in.

$a_{f2} = -.3129$ lb. sec.^{2}/in.

$a_{f3} = 5.912 \times 10^{-5}$ lb. sec.^{3}/in.

$$k_f(\text{rear}) = a_{r0} + a_{r1}\dot{\phi} + a_{r2}\dot{\phi}^2 + a_{r3}\dot{\phi}^3 \qquad (3)$$

$a_{r0} = 1.321 \times 10^6$ lb./in.

$a_{r1} = 81.28$ lb. sec./in.

$a_{r2} = -.1857$ lb. sec.^{2}/in.

$a_{r3} = 3.633 \times 10^{-5}$ lb. sec.^{3}/in.

Damping coefficients used in this study (arbitrarily) to account for dissipation at the forward and rear bearings are

$$c_f = 42. \text{ lb. sec./in.}$$
$$c_r = 31. \text{ lb. sec./in.} \tag{4}$$

A principal objective of the bearing design in the HPOTP is critical-speed-location control. The first two free-free bending modes (zero-bearing stiffnesses) for the rotating assembly of this turbopump are located at approximately 25,570 and 58,170 rpm. Because of the comparatively stiff bearing design (and gyroscopic stiffening), the calculated critical speeds of the turbopump lie at approximately 13,000 and 40,000 rpm. Hence, the operating speed range of the turbopump (20,890 to 31,160 rpm.) is well removed from the rotor's critical speeds.

The balance procedure presently planned for the HPOTP consists of the following steps:

a. The rotating assembly is balanced at low speed in a balance assembly.

b. The rotating assembly is then partially disassembled prior to reassembly in the turbopump.

On the basis of past experience with similar turbopumps, Rocketdyne personnel* suggest that <u>reasonable</u> values for residual turbopump imbalance would be the following:

a. 1 gm. in. at the boost stage impeller,

b. 5 gm. in. at the main impeller, and

c. 5 gm. in. at the turbines.

---

*Personal communication with B. Rowan, 6/2/73.

The orientation of the rotor imbalances relative to either one another or the rotor is not predictable.

At the present time, Rocketdyne plans to measure the transient motion of the rotor with five radially mounted and two axially mounted Bently proximity gauges. The planned radial Bently locations are as follows:

a. Immediately behind the boost stage impeller, and approximately 2.6 in. from the front of the rotating assembly,

b. Immediately behind the inboard front bearing, and approximately 5.4 in. from the front of the rotating assembly,

c. At the forward inlet of the main stage impeller, and approximagely 7.6 in. from the front of the rotating assembly,

d. Immediately forward of the inboard rear bearing, and approximately 13.9 in. from the front of the rotating assembly, and

e. Forward of the inboard hot-gas turbine, and approximately 20.13 in. from the front of the rotating assembly.

The axial Bently's are to be located at the rear of the boost and mainstage impellers.

HPOTP Structural Dynamic Properties

The structural dynamic analysis for a turbopump is initiated by modeling its rotating assembly as a collection of rigid bodies connected by a massless elastic structure. Rocketdyne's structural dynamic model of the HPOTP employs 13 rigid bodies connected by either uniform or discontinuous beam structures. Each rigid body has both a displacement and a rotational degree of freedom. The

inertia properties of the rigid bodies, together with their location relative to the mass center of the rotating assembly, are provided in Table 1. The entries $m_i, J_i, \bar{J}_i$ are the mass, diametral, and polar moments of inertia of the ith component rigid body. The $a^i_{\bar{x}}, a^i_{\bar{y}}, a^i_{\bar{z}}$ entries in Table 1 are the coordinates of the component rigid bodies in the $\bar{x}, \bar{y}, \bar{z}$ coordinate system. The origin of the $\bar{x}, \bar{y}, \bar{z}$ system coincides with the rotating assembly mass center. The $a^i_{\bar{z}}$ component defines the axial position of the rigid bodies with positive $\bar{z}$ being directed towards the turbine. The $a^i_{\bar{x}}$ and $a^i_{\bar{y}}$ components define the eccentricity (imbalance) of component rigid bodies. The magnitude and axial location of the imbalance distribution defined in Table A.1 is consistent with Rocketdyne estimates; however, the orientation of the imbalance with respect to the $\bar{x}, \bar{y}, \bar{z}$ system is arbitrary. The rigid body properties of the HPOTP follow

$$
\begin{aligned}
m &= .1966 \text{ lb. sec.}^2/\text{in.} \\
J &= J_{\bar{x}} = J_{\bar{y}} = 9.968 \text{ lb. sec.}^2 \text{ in.} \\
\bar{J} &= J_{\bar{z}} = 1.212 \text{ lb. sec.}^2 \text{ in.} \\
J_{\bar{x}\bar{z}} &= -5.104 \times 10^{-3} \text{ lb. sec.}^2 \text{ in.} \\
J_{\bar{y}\bar{z}} &= -1.435 \times 10^{-3} \text{ lb. sec.}^2 \text{ in.} \\
a_{\bar{x}} &= 4.358 \times 10^{-3} \text{ in.}, \quad a_{\bar{y}} = 1.4526 \times 10^{-3} \text{ in.}
\end{aligned}
\tag{5}
$$

where m is the rotor mass and J and $\bar{J}$ are the rigid body diametral and polar moments of inertia. Further, the components $a_{\bar{x}}$, $a_{\bar{y}}$ define rigid body imbalance and $J_{\bar{x},\bar{z}}$, $J_{\bar{y}\bar{z}}$ are the rigid body products of inertia which result from the imbalance distribution of Table 1.

The results of eigenanalysis performed by Rocketdyne which are pertinent to this investigation are the lowest two (non-zero) free-free eigenvalues and their associated eigenvectors. The two lowest free-free natural frequencies follow

$$\lambda_1 = 2{,}677.8 \text{ rad./sec.} = 25{,}584 \text{ rpm.}$$
$$\lambda_2 = 6{,}091.9 \text{ rad./sec.} = 58{,}203 \text{ rpm.} \qquad (6)$$

An eigenvector for the rotor includes both the displacement and rotational degrees of freedom for each component body. These eigenvectors are presented in partitioned form in Table 2 where $[A_e]$ contains the displacements and $[A_\beta]$ the rotational degrees of freedom. The eigenvectors are normalized to satisfy the following orthogonality condition

$$[A_e]^T[m][A_e] + [A_\beta]^T[J][A_\beta] = [U] \qquad (7)$$

where $[m]$ and $[J]$ are diagonal matrices whose elements are m_i and J_i. The superscript T in Eq. (7) defines the matrix transpose operation, and $[U]$ is the unity matrix. Stations 2, 6, 8, 11, and 17 of Table 2 correspond to axial positions for which Bently proximity gauges are planned. These station locations were not included in Rocketdyne's original structural dynamic model. The entries in Table 2 for these station locations were obtained via linear interpolation between adjacent stations.

	a_z^i	$m_i \times 10^3$	$J_i \times 10^3$	$\bar{J}_i \times 10^3$	$a_x^i \times 10^3$	$a_y^i \times 10^3$
1.	-12.75	8.67	10.61	16.92	0.659	0.0
2.	-11.70	6.36	4.672	8.284	0.0	0.0
3.	-10.69	2.24	0.833	1.314	0.0	0.0
4.	-9.82	1.79	0.618	1.055	0.0	0.0
5.	-8.19	7.47	5.976	6.620	0.0	0.0
6.	-5.02	62.1	228.2	257.7	0.0	0.460
7.	-1.42	9.34	8.967	8.560	0.0	0.0
8.	.126	3.55	1.927	1.927	0.0	0.0
9.	1.25	5.74	3.666	3.665	0.0	0.0
10.	2.31	6.64	7.213	7.212	0.0	0.0
11.	3.75	7.81	8.079	8,079	0.0	0.0
12.	5.48	4.69	30.99	3.099	0.0	0.0
13.	7.63	70.2	508.8	508.8	0.407	0.0

TABLE 1. Geometric and inertial data for the SSME HPOTP

	a_z^i	$[A_e]$ matrix		$[A_\beta]$ matrix	
1.	-12.75	5.112	3.965	1.025	1.495
2.	-12.06	4.401	2.915	1.023	1.486
3.	-11.70	4.032	2.369	1.022	1.480
4.	-10.69	2.983	.8182	.9998	1.384
5.	-9.82	2.106	-.4005	.9548	1.199
6.	-9.25	1.595	-.9250	.8628	.8493
7.	-8.19	.6602	-1.886	.6943	.2077
8.	-7.00	-.0528	-1.877	.6401	.0384
9.	-5.02	-1.221	-1.861	.5514	-.2391
10.	-1.42	-2.771	.0513	.0381	-.5219
11.	-.749	-2.698	.4687	-.0598	-.4980
12.	.126	-2.604	1.009	-.1865	-.4671
13.	1.25	-2.340	1.573	-.2738	-.3709
14.	2.31	-1.998	1.972	-.3523	-.2337
15.	3.75	-1.397	2.236	-.4534	.0223
16.	5.48	-.4504	1.921	-.5891	.4973
17.	5.50	-.4304	1.903	-.6090	.6428
18.	7.63	.9311	.377	-.6614	.9092

TABLE 2. HPOTP rotating assembly eigenvectors

Simulation Procedure and Results

The output capability of the simulation model is summarized below.

1. Bearing motion. The transient motion of the shaft at bearing locations is generated. Bearing motion output includes both the motion of the shaft in two orthogonal planes as a function of time and X-Y plots of shaft orbital motion, i.e., the output corresponds to the shaft motion which would be observed from either a side or axial view of the rotor. Solutions are generated for the forward-inboard and rear-outboard bearings.
2. Modal coordinates. The transient solution of modal coordinates associated with the two free-free rotor bending modes are generated. These solutions are of interest in verifying the correctness of the model's operation, but are not significant from a turbopump operational viewpoint.
3. Bearing reactions. The resultant reactions for forward-inboard and rear-outboard reactions are generated as a function of time.
4. Spin velocity. The rotor spin velocity in rpm. is generated as a function of time.
5. Spin acceleration. The rotor spin acceleration in rad./sec.^{2} is generated as a function of time.
6. Simulated Bently output. Motion of the rotor is generated for axial positions along the shaft corresponding to planned Bently proximity gauge locations. Radial motion in two orthogonal planes is defined with both time and X-Y solutions.

7. Maximum shaft deflections. Plots of radial shaft-deflection magnitudes as a function of rotor axial position are generated periodically. The following procedure is followed in obtaining these plots. At each time t_i in the simulation, a vector is generated whose components are the shaft-deflection magnitudes $w_j(t_i)$ at j rotor axial stations. The maximum of the j rotor deflection magnitudes $w_j(t_i)$, denoted $W(t_i)$, is calculated. A search is made over 100 succeeding values of t_i for the maximum value of $W(t_i)$, denoted $W(t_i*)$. The plots of maximum shaft deflection magnitudes provided correspond to the $w_j(t_i^*)$ vectors. In other words, a plotted shaft-deflection-magnitude vector includes the maximum rotor deflection magnitude over the time of observation.

The validity of a transient simulation model is primarily established by the degree to which the model correctly identifies the location and form of rotor critical speeds. As noted previously the critical speed locations calculated by Rocketdyne for the HPOTP rotating assembly are approximately 13,000 and 40,000 rpm. The transient model correctly identifies both the critical speed locations and the deflection mode shape of the rotor during transition through the critical speed.

From a rotordynamic viewpoint, the most severe operating conditions for the HPOTP arise during transition through the first critical speed and during steady-state operation at emergency power levels. Considering the critical speed transition first, the amplitude of transient rotor deflections largely

depends on the rate at which the rotor is accelerated (or decelerated) through the critical speed and the damping which is present. The proposed system operation of the SSME is such that the critical-speed transition during startup is considerably more rapid than at shutdown; hence, the shutdown transition was examined. The rate of deceleration of the rotor in the vicinity of the first critical speed (6) during shutdown is approximately 940 rad./sec.^{2} while the comparable value during startup is 3660 rad./sec.^{2}

Damping is provided in the rotor model by modal damping in the rotor and by concentrated damping at the bearings. The modal damping factors used in this study were two percent of critical. This value is felt to be conservative. Damping at the bearings is accounted for by linear damping coefficients which would correspond to the physical model of a dashpot attached between the turbopump housing and the rotating assembly. There is a great deal of uncertainty involved in the amount of damping provided by the ball bearings and the fluid surrounding the turbopump rotating assembly. The damping factors used in this study yield a rapid attentuation of initial starting transients, and are felt to reasonably account for external rotor damping.

Figure 4 illustrates some of the results of a transition through the 13,000 rpm. critical speed. The rotor is decelerated from 13,380 to 12,500 rpm. at a nominal deceleration rate of 940 rad./sec.^{2}. The results of the separate frames of figure 4 are discussed below.

Figures 4(a), (b), and (c) illustrate the motion of the shaft at the turbine floating-ring seal location. Figures (a), and (b) illustrate the shaft-deflection time history in the orthogonal X-Y and Y-Z planes where the Z axis defines the nominal geometric axis of the turbopump, i.e., these solutions correspond to the motion which would be observed by looking in at the shaft radially. By contrast, the solution presented in figure (c) corresponds to the motion which would be observed from an axial position. The steady-state biased displacement of the rotor displayed in figures 4(a) and (c) results from the hydrodynamic side loads, which are applied to the turbopump in the X-Z plane.

Figures 4(d) through (h) illustrate the maximum shaft magnitudes experienced during initial-speed transition. A better appreciation of this figure is obtained by noting that the magnitude (absolute value) of deflection is plotted. The * markings on the plot denotes either a station location in Rocketdyne's structural dynamic model or a planned Bently location. The forward bearings on the turbopump are located at -10.7 and -9.8 inches, the rear bearings are located at .12 and 1.24 inches, and the extreme right-hand station corresponds to a location between the turbine wheels. The figure basically illustrates that large deflections are the results of the overhung turbine wheel design. The deflections in the neighborhood of 5.5 in. are sufficient to cause rubbing on the turbine floating ring seals. The clearance at this location is .005 in. and the predicted

deflections are .010 in. Time solutions for the deflections at this location were provided in figures 4(a), (b), and (c).

The operating conditions and physical-parameters which were used in the simulation model to obtain a rubbing condition at the turbine-floating-ring seals are not worst case. Specifically, the imbalance distribution, the damping and the time interval required for critical-speed transition could all be worse than those used here with a consquent increase in deflections. The imbalance distribution of Table 1 was not chosen to maximize the rotor deflections. For example, larger deflection amplitudes could be obtained from the following distribution

$$a_{\bar{x}}^{1} = .659 \times 10^{-3} \text{ in.}, \; a_{\bar{x}}^{6} = -.960 \times 10^{-3} \text{ in.}, \; a_{\bar{x}}^{13} = .907 \times 10^{-3} \text{ in.}$$

with all other $a_{\bar{x}}^{i}$, $a_{\bar{y}}^{i}$ zero. The two percent of critical damping factors used to model structural damping of the rotating assembly could conceivably be half percent or less. A simulation run was made in which a 100-lb. step increase in side loading was imposed on the rotating assembly (at zero running speed). The resultant damping factor was approximately 3.5 percent of critical. The same type of run was made at a running speed slightly above the critical speed location, and the motion due to the disturbance was completely absent from the plots after 4 cycles demonstrating that the model is not lightly damped. The deceleration rate through the critical speed used here was 940 rad./sec.^{2}, which is the predicted (6) rate between 14,000 and 13,000 rpm. However, the predicted deceleration rate for less than 13,000 rpm. is

approximately 520 rad./sec.^{2} Hence, the deflections predicted in this study are considered to be reasonable, and a possibility exists for larger and potentially more damaging amplitudes.

The transient response of the modal coordinates $\mathcal{F}^1_{\bar{x}}, \mathcal{F}^2_{\bar{x}}$ are illustrated in figures 4(i) and (j). The peak magnitudes of these functions coincide (in time) with the shaft motion of figures 4(a) and (b). The amplitude of $\mathcal{F}^1_{\bar{x}}$ is seen to be an order of magnitude larger than that of $\mathcal{F}^2_{\bar{x}}$. The <u>elastic</u> deflections of the rotor are defined in the rotor-fixed $\bar{x}$, $\bar{y}$, $\bar{z}$ coordinate system as a linear summation of the modal coordinates. The oscilliation in these coordinates at the running speed frequency results from the hydrodynamic side loads. The combined effects of rotor imbalance and the critical-speed transition account for the comparatively slow oscillation in these variables.

The rotor spin acceleration is illustrated in figure 4(k). This solution is included to demonstrate the coupling of the transverse oscillations to the spin-axis motion. This feature of the simulation model is of no particular value in the present (high-spin acceleration) application. However, it is required to correctly simulate a "slow", power-limited, cirtical-speed transition.

Although not illustrated, the peak reactions for forward and rear bearings are approximately 220 and 450 lbs., respectively. This magnitude of transient bearing loads does not constitute a problem.

A simulation run was executed to examine the motion of the turbopump at EPL, which corresponds to $\dot{\phi}$ = 31,140 rpm. The

results basically resemble those presented in figure 4. Figure 5 illustrates a shaft deflection magnitude plot for EPL conditions, and demonstrates, that shaft deflections are generally less than .002 in. The maximum bearing loads on the forward and rear bearings at EPL are approximately 750 and 650 lbs., respectively. The results of the HPOTP simulation runs for EPL conditions do not indicate any problem areas associated with either excessive shaft deflections or excessive bearing loads.

CONCLUDING COMMENTS

The results of this study indicate no problems in operating the HPOTP at EPL conditions. However, the results indicate a potentially serious problem during critical-speed transition at shutdown. Specifically, for the presently projected rotor deceleration rate and imbalance distribution, a rubbing condition at the turbine floating-ring seals is predicted. The problem can be reduced to some extent by reducing the imbalance at the HPOTP turbine wheels. The problem would also be reduced if the rotor were decelerated through the critical speed more rapidly, or if additional damping were provided.

This study resulted from the cooperative assistance of both NASA and Rocketdyne personnel, and (to the author's knowledge) represents the first use of a general purpose, transient, flexible-rotor simulation model as a development tool in a liquid-rocket-engine program prior to hardware testing. This study was conducted to anticipate and avoid hardware failures. By contrast, simulation efforts in the past have resulted from (sometimes catastrophic) hardware failures, and have been hampered by ad hoc models of limited capability. The results of this study have indicated a potentially serious operational problem well in advance of operational turbopump testing. Time has accordingly been purchased for a careful analysis of alternative hardware and operational adjustments. Time has also been purchased in the design of the turbopump test program to verify the effectiveness of such adjustments.

REFERENCES

1. D. W. Childs, "Transient Rotordynamic Analysis for the Space Shuttle Main Engine High-Pressure Turbopumps", Final Report, 1973 NASA-ASEE summer Faculty Fellowship Research Program, University of Alabama, September 1973.

2. D. W. Childs, "A Rotor-Fixed Simulation Model for Flexible Rotating Equipment," Paper No. 73-DET-123, ASME Vibration Conference, Cincinnati, Ohio, September 1973.

3. Jones, A. B., "A General Theory for Elastically Constrained Ball and Radial Roller Bearings Under arbitrary Load and Speed Conditions," ASME Journal of Basic Engineering, Vol. 82, No. 2, pp. 309-320, June 1960.

4. Jones, A. B., "Ball Motion and Sliding Friction in Ball Bearings," ASME Journal of Basic Engineering, Vol. 82, No. 1, pp. 1-12.

5. Anon., Engine Design Definition Report - TURBOMACHINERY, RSS-8502-4, DRD-SE-275, SSME PHASE CD/NAS8-26187/4-21-71.

6. Sack, L., SSME Preliminary Design Review Data Dump, Rocketdyne Division Rockwell International, Canoga Park, California, 28 July 1972.

APPENDIX A

THE SIMULATION MODEL

Kinematics

A modal simulation model from Ref. [2] was employed in this study. The rigid body kinematics required are illustrated in figure A.1. The $\bar{x}$, $\bar{y}$, $\bar{z}$ coordinate system of this figure is fixed in the elastic rotor, and its origin coincides with the rotor's mass center. The $\bar{z}$ axis coincides with the nominal rotational axis of symmetry of the rotor. The vector R locates the mass center of the rotor in the inertial X, Y, Z system, and Ω is the angular velocity of the $\bar{x}$, $\bar{y}$, $\bar{z}$ system relative to the X, Y, Z system. The orientation of the $\bar{x}$, $\bar{y}$, $\bar{z}$ system relative to the X, Y, Z system is defined by the Euler angle set α_1, α_2, ϕ. The constraints of the bearings on rotor motion justifiy the customary "small" angle assumption for α_1 and α_2, i.e.,

$$\begin{aligned} \dot{\alpha}_1 &= (\Omega_{\bar{x}} c\phi - \Omega_{\bar{y}} s\phi)/c\alpha_2 \cong \Omega_{\bar{x}} c\phi - \Omega_{\bar{y}} s\phi \\ \dot{\alpha}_2 &= \Omega_{\bar{x}} s\phi + \Omega_{\bar{y}} c\phi \\ \dot{\phi} &= \Omega_{\bar{z}} - \dot{\alpha}_1 s\alpha_2 \cong \Omega_{\bar{z}} \end{aligned} \tag{A.1}$$

where $c\phi = \cos\phi$, $s\phi = \sin\phi$, etc.

The operation of differentiation with respect to time in the various coordinate systems is defined in terms of the arbitrary vector v as follows:

$\dot{v} = \frac{dv}{dt}\Big|_{X,Y,Z}$ = the time rate of change of the vector v as seen by an observer fixed in inertial space

$\bar{\dot{v}} = \frac{dv}{dt}\Big|_{\bar{x},\bar{y},\bar{z}}$ = the time rate of change of the vector v as seen by an observer fixed in the $\bar{x}$, $\bar{y}$, $\bar{z}$ system.

The components of vectors are required in both the X, Y, Z and $\bar{x}$, $\bar{y}$, $\bar{z}$ system, and the following notation is defined in terms of the arbitrary vector v

$(v)_I$: implies components in X, Y, Z system

$(v)_i$: implies components in $\bar{x}$, $\bar{y}$, $\bar{z}$ system

The following orthogonal coordinate transformation relating these components is required:

$$(v)_i = [A](V)_I ,$$

where to a comparable level of accuracy with Eq. (1)

$$[A] = \begin{matrix} c\phi & s\phi & -\alpha_2 c\phi + \alpha_1 s\phi \\ -s\phi & c\phi & \alpha_2 s\phi + \alpha_1 c\phi \\ \alpha_2 & -\alpha_1 & 1 \end{matrix} \qquad (A.2)$$

The rotor's distributed parameter character is accounted for by an n-body lumped parameter approximation. The position of the ith rigid body relative to the $\bar{x}$, $\bar{y}$, $\bar{z}$ coordinate system is defined by the vector r^i illustrated in figure A.2. The vector e^i defines the elastic displacement of the origin of the $\tilde{x}_i$, $\tilde{y}_i$, $\tilde{z}_i$ system. The angular orientation of the body-fixed $\tilde{x}_i$, $\tilde{y}_i$, $\tilde{z}_i$ system relative to the x_i, y_i, z_i system (and $\bar{x}$, $\bar{y}$, $\bar{z}$ system) is defined by the Euler angle set $\beta^i_{\bar{x}}$, $\beta^i_{\bar{y}}$, $\beta^i_{\bar{z}}$ which are analgous in their order of rotation to the Euler angle set α_1, α_2, ϕ illustrated in figure A.1(b). Axial and torsional elastic deflections are neglected in this analysis; hence, the elastic deflections of the rotor are defined in the $\bar{x}$-$\bar{z}$ and $\bar{y}$-$\bar{z}$ planes by the vectors

$$(e_{\bar{x}})^T = (e^1_x, e^2_x, ..e^n_x) \quad , \quad (\beta_{\bar{y}})^T = (\beta^1_y , \beta^2_y, ...\beta^n_y)$$
$$(e_{\bar{y}})^T = (e^1_y , e^2_y, ...e^n_y) \quad , \quad (\beta_{\bar{x}})^T = (\beta^1_x , \beta^2_x, ...\beta^n_x) \qquad (A.3)$$

where the superscript T denotes the matrix transpose operation.

The free-free bending modes (eigen-vectors) of the rotor are used to define the following orthogonal transformation and to introduce modal coordinates

$$(e_{\bar{x}}) = [A_e](q_{\bar{x}}) \quad , \quad (\beta_{\bar{y}}) = [A_\beta](q_{\bar{x}})$$
$$(e_{\bar{y}}) = [A_e](q_{\bar{y}}) \quad , \quad (\beta_{\bar{x}}) = -[A_\beta](q_{\bar{y}}) \tag{A.4}$$

The matrices $[A_e]$, $[A_\beta]$ satisfy

$$[A_e]^T(m) = 0 \ , \ [A_e]^T(ma_{\bar{z}}) + [A_\beta]^T(J) = 0 \tag{A.5}$$

In addition, they are normalized to satisfy the orthogonality relationship

$$[A_e]^T(m)[A_e] + [A_\beta]^T[J][A_\beta] = [U] \tag{A.6}$$

where [U] is the unity matrix. In Eq. (A.5), the elements of the vectors (m), $(ma_{\bar{z}})$, and (J) are m_i, $m_i a^i_{\bar{z}}$, and J^i, respectively, where

m_i = mass of component rigid body i.

J^i = diametral moment of inertia of component rigid body i.

a^i_z= nominal axial position of the mass center of component rigid body i.

The output variables of primary interest from a rotor simulation model are the displacements w^i and velocities $\dot{w}^i$ of the bearings and of component rigid bodies. The displacement of a component rigid body can be defined by the vector equation

$$w^i = R - b^i + a^i + e^i$$

where b^i locates the initial position of the ith component rigid body in the X, Y, Z system, and a^i locates its nominal position in the x, y, z system. The vector definition for the velocity of the rigid body in the X, Y, Z system is

$$\dot{w}^i = \dot{R} + \dot{\bar{e}}^i + \Omega \times (a^i + e^i)$$

The component statement of these equations is

$$(w^i)_I = (R)_I - (b^i)_I + [A]^T(a^i + e^i)_{\bar{i}}$$
$$(\dot{w}^i)_I = (\dot{R})_I + [A]^T\{(\dot{\bar{e}}^i)_{\bar{i}} + [(\Omega)_{\bar{i}}](a^i + e^i)_{\bar{i}}\} \quad , \tag{A.7}$$

where the notation $[(\Omega)_{\bar{i}}]$ implies

$$[(\Omega)_{\bar{i}}] = \begin{matrix} 0 & -\Omega_{\bar{z}} & \Omega_{\bar{y}} \\ \Omega_{\bar{z}} & 0 & -\Omega_{\bar{x}} \\ -\Omega_{\bar{y}} & \Omega_{\bar{x}} & 0 \end{matrix}$$

and performs the matrix equivalent of the vector cross product operation. From Eq. (A.4), one obtains the definitions

$$(e_{\bar{x}}) = [A_e](q_{\bar{x}}) \quad , \quad (\dot{\bar{e}}_{\bar{x}}) = [A_e](\dot{q}_{\bar{x}})$$
$$(e_{\bar{y}}) = [A_e](q_{\bar{y}}) \quad , \quad (\dot{\bar{e}}_{\bar{y}}) = [A_e](\dot{q}_{\bar{y}}) \tag{A.8}$$

Eqs. (A.7) and (A.8) can be used to calculate the displacements and velocities of each component rigid body.

This completes the required kinematics for the governing equations of motion. The vectors R and Ω, and the Euler angles α_1, α_2, ϕ are used to define the location and orientation of the $\bar{x}$, $\bar{y}$, $\bar{z}$ coordinate system, while the modal coordinates $(q_{\bar{x}})$, $(q_{\bar{y}})$ define the elastic deflections of the component rigid bodies relative to the $\bar{x}$, $\bar{y}$, $\bar{z}$ system.

Equations of Motion

The modal vibration equations for the $\bar{x}$-$\bar{z}$ and $\bar{y}$-$\bar{z}$ planes are

$$(\ddot{q}_{\bar{x}}) = (F_{\bar{x}}) + \dot{\phi}\{2[U]-[CM]\}(\dot{q}_{\bar{y}}) - \{[\Lambda] + \dot{\phi}^2[CK]\}(q_{\bar{x}})$$
$$+\ddot{\phi}[CK](q_{\bar{y}}) + \dot{\phi}\Omega_{\bar{x}}(c_v) + (GF)_{\bar{x}} \tag{A.9}$$
$$(\ddot{q}_{\bar{y}}) = (F_{\bar{y}}) - \dot{\phi}\{2[U]-[CM]\}(\dot{q}_{\bar{x}}) - \{[\Lambda] + \dot{\phi}^2[CK]\}(q_{\bar{y}})$$
$$+\ddot{\phi}[CK](q_{\bar{x}}) + \dot{\phi}\Omega_{\bar{y}}(c_v) + (GF)_{\bar{y}}$$

In the above, $[\Lambda]$ is the diagonal matrix of free-free (non-zero) eigenvalues. The vectors $(F_{\bar{x}})$ and $(F_{\bar{y}})$ are generalized modal force vectors defined by

$$(F_{\bar{x}}) = [A_e]^T(f_{\bar{x}}) + [A_\beta]^T(M_{\bar{y}})$$
$$(F_{\bar{y}}) = [A_e]^T(f_{\bar{y}}) - [A_\beta]^T(M_{\bar{x}})$$

where

$$(f_{\bar{x}})^T = (f^1_{\bar{x}},\ f^2_{\bar{x}}\ ,\ \ldots\ f^n_{\bar{x}})\ ,\ (M_{\bar{y}})^T = (M^1_{\bar{y}},\ M^2_{\bar{y}},\ \ldots\ M^n_{\bar{y}})$$
$$(f_{\bar{y}})^T = (f^1_{\bar{y}},\ f^2_{\bar{y}}\ ,\ \ldots\ f^n_{\bar{y}})\ ,\ (M_{\bar{x}})^T = (M^1_{\bar{x}},\ M^2_{\bar{x}},\ \ldots\ M^n_{\bar{x}})$$

The vectors $(GF)_{\bar{x}}$ and $(GF)_{\bar{y}}$ define the modal forcing functions due to distributed imbalance and asymmetry, and are defined by

$$(GF)_{\bar{x}} = [Z](gf)_{\bar{x}}\ ,\ (GF)_{\bar{y}} = [Z](gf)_{\bar{y}} \tag{A.10}$$

where

$$(gf)_{\bar{x}} = \begin{matrix} \dot{\phi}^2 \\ \ddot{\phi} \\ \dot{\phi}^2 \\ \ddot{\phi} \end{matrix}\ ,\quad (gf)_{\bar{y}} = \begin{matrix} -\ddot{\phi}^2 \\ \dot{\phi}^2 \\ -\ddot{\phi} \\ \dot{\phi}^2 \end{matrix}$$

and

$$[Z] = [(z^1)(z^2)(z^3)(z^4)]$$
$$= [\ [A_e]^T(ma_{\bar{x}}),\ [A_e]^T(ma_{\bar{y}}),\ [A_\beta]^T(J^o_{\bar{x}\bar{z}}),\ [A_\beta]^T(J^o_{\bar{y}\bar{z}})] \tag{A.11}$$

The components of the vectors $(ma_{\bar{x}})$, $(ma_{\bar{y}})$, $(J^o_{\bar{x}\bar{z}})$, $(J^o_{\bar{y}\bar{z}})$ are $m_i a^i_{\bar{x}}$, $m_i a^i_{\bar{y}}$, $J^{io}_{\bar{x}\bar{z}}$, $J^{io}_{\bar{y}\bar{z}}$, respectively, where

$a^i_{\bar{x}}$, $a^i_{\bar{y}}$ = eccentricity of component rigid body i.

$J^{io}_{\bar{x}\bar{z}}$, $J^{io}_{\bar{y}\bar{z}}$ = product of inertias of component rigid body i in the body-fixed x_i, y_i, z_i coordinate system.

Returning to Eq. (A.7),

$$[CM] = [A_\beta]^T[J][A_\beta]$$
$$[CK] = [A_\beta]^T[\bar{J}-J][A_\beta] - [A_e]^T[m][A_e] = [CM] - [U] \tag{A.12}$$
$$(c_v) = [A_\beta]^T(\bar{J}),\ (\bar{J})^T = (\bar{J}^1,\ \bar{J}^2,\ \ldots\ \bar{J}^n)$$

where $[\bar{J}]$ and $[\bar{J}-J]$ are diagonal matrices whose entries are $\bar{J}_i$ (polar moment of inertia of component rigid body i) and $\bar{J}_i - J_i$, respectively.

The defining equations of motion for the "rigid-body" variables R, Ω are

$$(F^r)_I = m(\ddot{R})_I \tag{A.13}$$

$$(M^r)_{\bar{i}} = [J_{\bar{i}}](\dot{\Omega})_{\bar{i}} + [(\Omega)_{\bar{i}}][J^o{}_{\bar{i}}](\Omega)_{\bar{i}} \tag{A.14}$$

$$\begin{aligned} &\dot{\phi}(c_v)^T\{(\dot{q}_{\bar{x}}) + \dot{\phi}(q_{\bar{y}})\} \\ &+ \dot{\phi}(c_v)^T\{(\dot{q}_{\bar{y}}) - \dot{\phi}(q_{\bar{x}})\} \\ &\qquad P_{\bar{z}} \end{aligned}$$

where F^r and M^r are the resultant external forces and moments acting on the body, and

$$\begin{aligned} P_{\bar{z}} = {} & 2\dot{\phi}\{(z^1)^T + (z^3)^T\}(\dot{q}_{\bar{x}}) + 2\dot{\phi}\{(z^2)^T + (z^4)^T\}(\dot{q}_{\bar{y}}) \\ & + \Omega_{\bar{x}}(c_v)^T\{(\dot{q}_{\bar{x}}) + (q_{\bar{y}})\} + \Omega_{\bar{y}}(c_v)^T\{(\dot{q}_{\bar{y}}) - \dot{\phi}(q_{\bar{x}})\} \end{aligned} \tag{A.15}$$

Returning to Eqs. (A.13) and (A.14), m is the total mass of the rotor, $[J^o{}_{\bar{i}}]$ is the aggregate "rigid body" moment of inertia for the rotor in the $\bar{x}$, $\bar{y}$, $\bar{z}$ system, and

$$[J_{\bar{i}}] = [J^o{}_{\bar{i}}] + \begin{matrix} 0 & 0 & (c_v)^T(q_{\bar{x}}) \\ 0 & 0 & (c_v)^T(q_{\bar{y}}) \\ (c_v)^T(q_{\bar{x}}) & (c_v)^T(q_{\bar{y}}) & 2\delta J_{\bar{z}\bar{z}} \end{matrix} \tag{A.16}$$

$$\delta J_{zz} = \{(z^1)^T + (z^3)^T\}(q_{\bar{x}}) + \{(z^2)^T + (z^4)^T\ (q_{\bar{y}})$$

LIST OF FIGURES

1. SSME HPOTP rotating assembly schematic.

2. Radial stiffness definition of the HPOTP rear bearing as a function of axial preload and shaft speed.

3. Radial stiffness definition of the HPOTP forward bearing and the HPFTP bearings as a function of axial preload and shaft speed.

4. Simulation model output for deceleration through 13,000 rpm. critical speed.

   (a-c) Motion of the rotor at the turbine floating-ring seal locations.

   (d-h) Maximum rotor deflection magnitudes along the shaft.

   (i) $q^1_{\bar{x}}$ modal coordinate response.

   (j) $q^2_{\bar{x}}$ modal coordinate response.

   (k) Spin acceleration, $\ddot{\phi}$, in rad./sec.^{2}

5. Maximum shaft deflection magnitudes at EPL.

   A.1 Rigid-Body Kinematics

   A.2 Kinematics for rigid-body i

Fig. 1. D.Childs

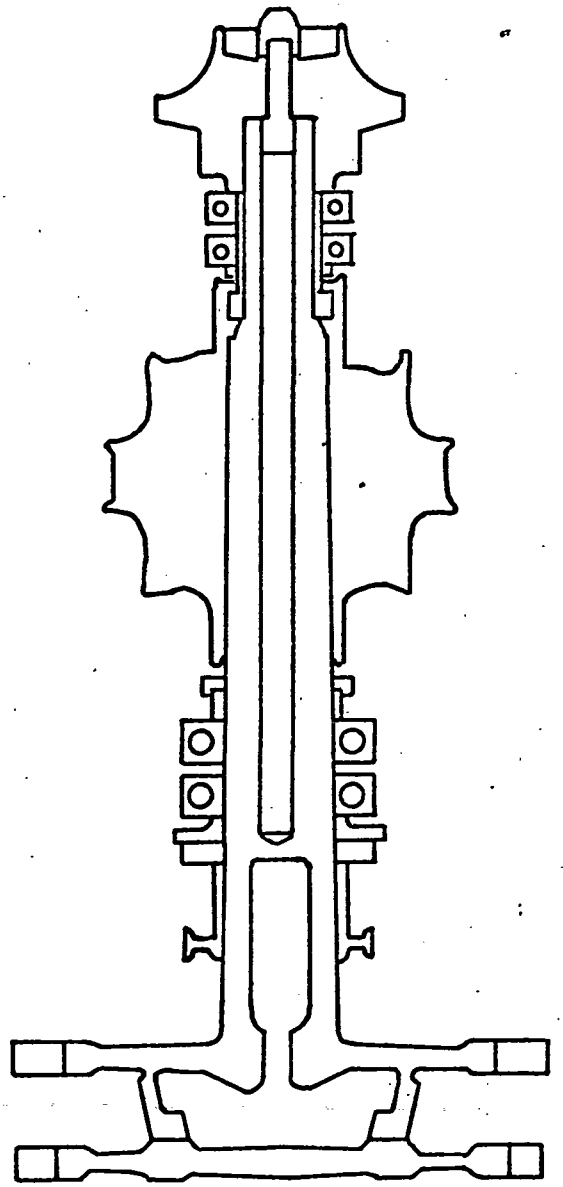

Fig. 2. D.Childs

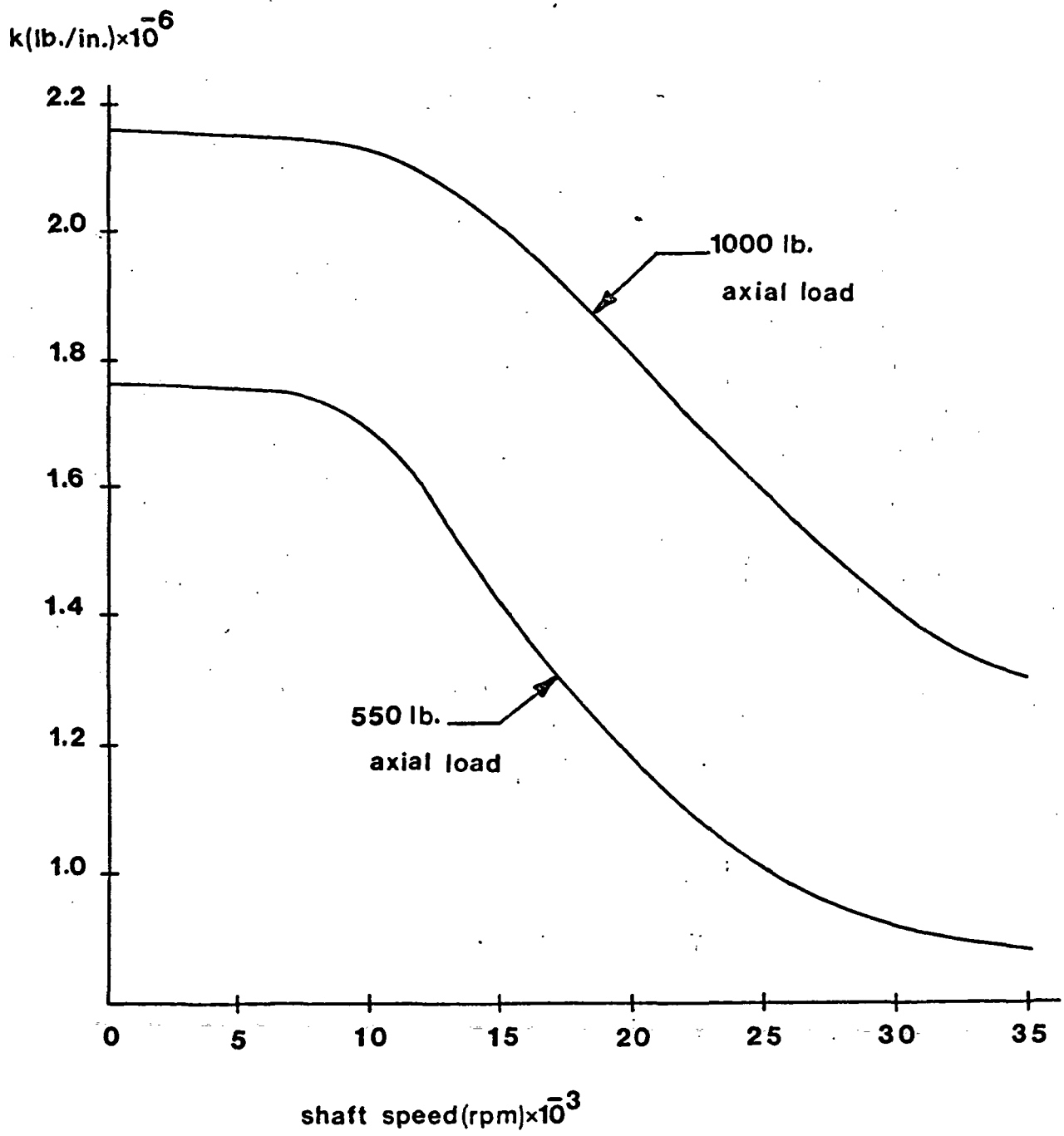

Fig. 3 D.Childs

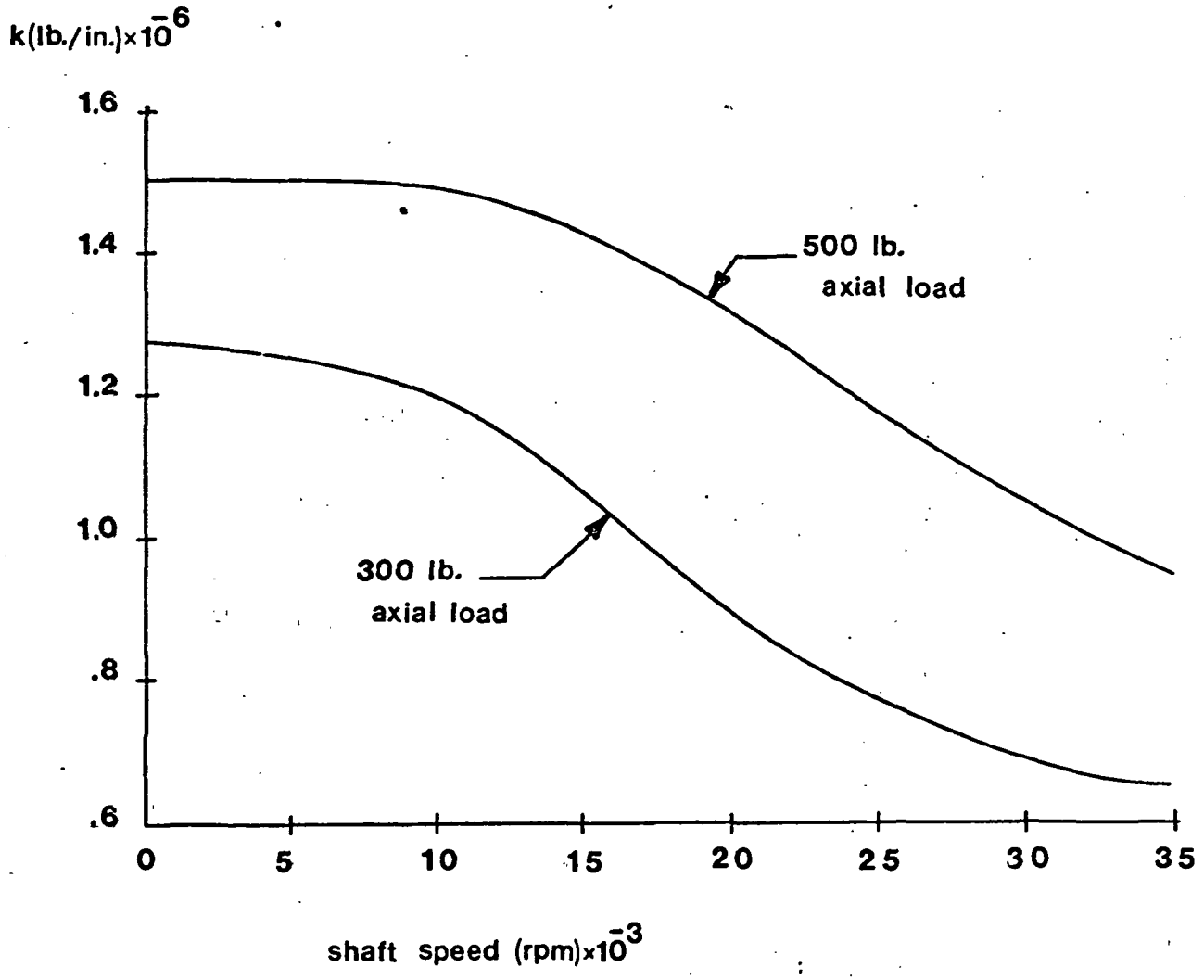

Figure 4(2). D. Childs

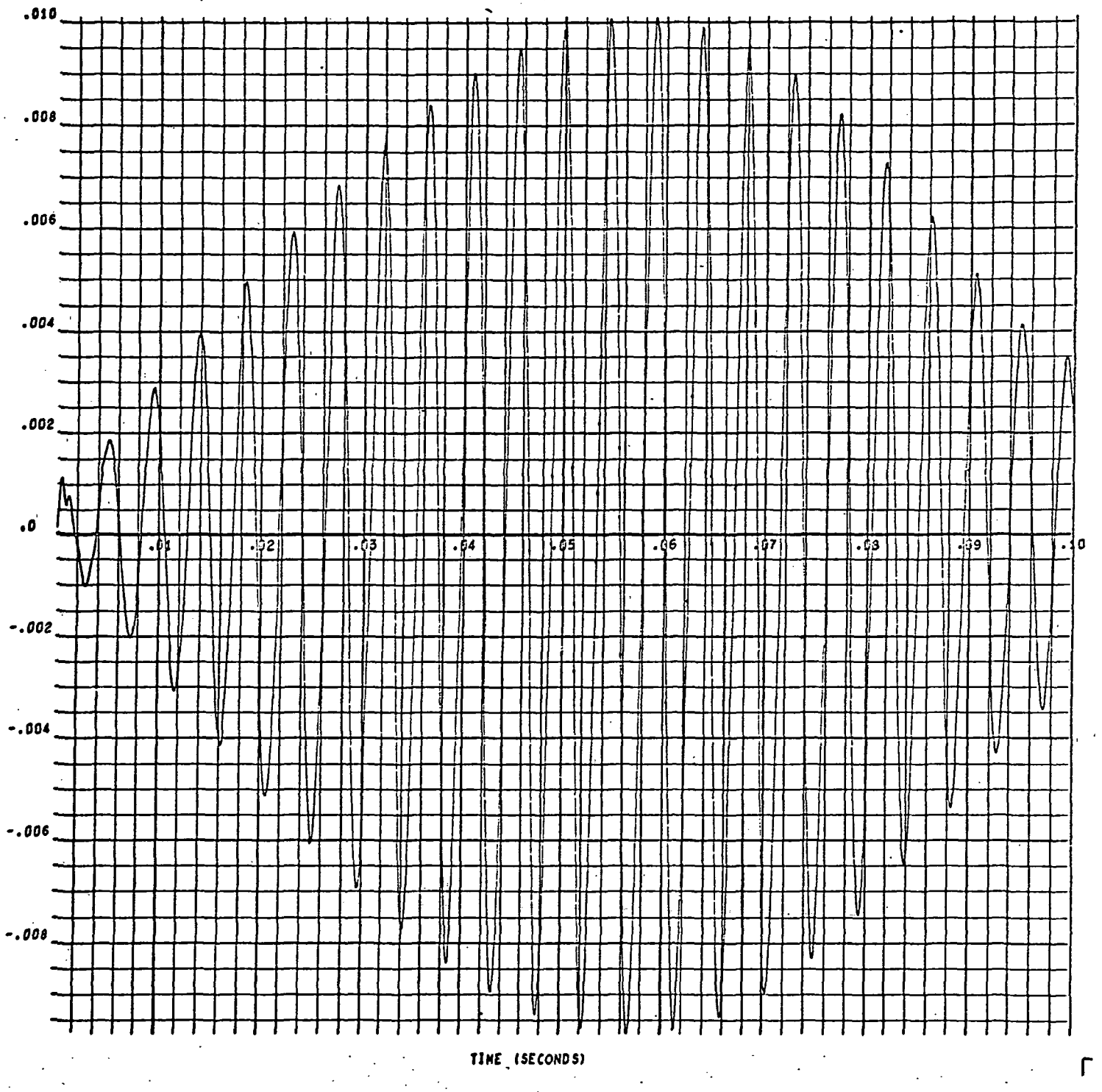

Figure 4(b) D. Childs

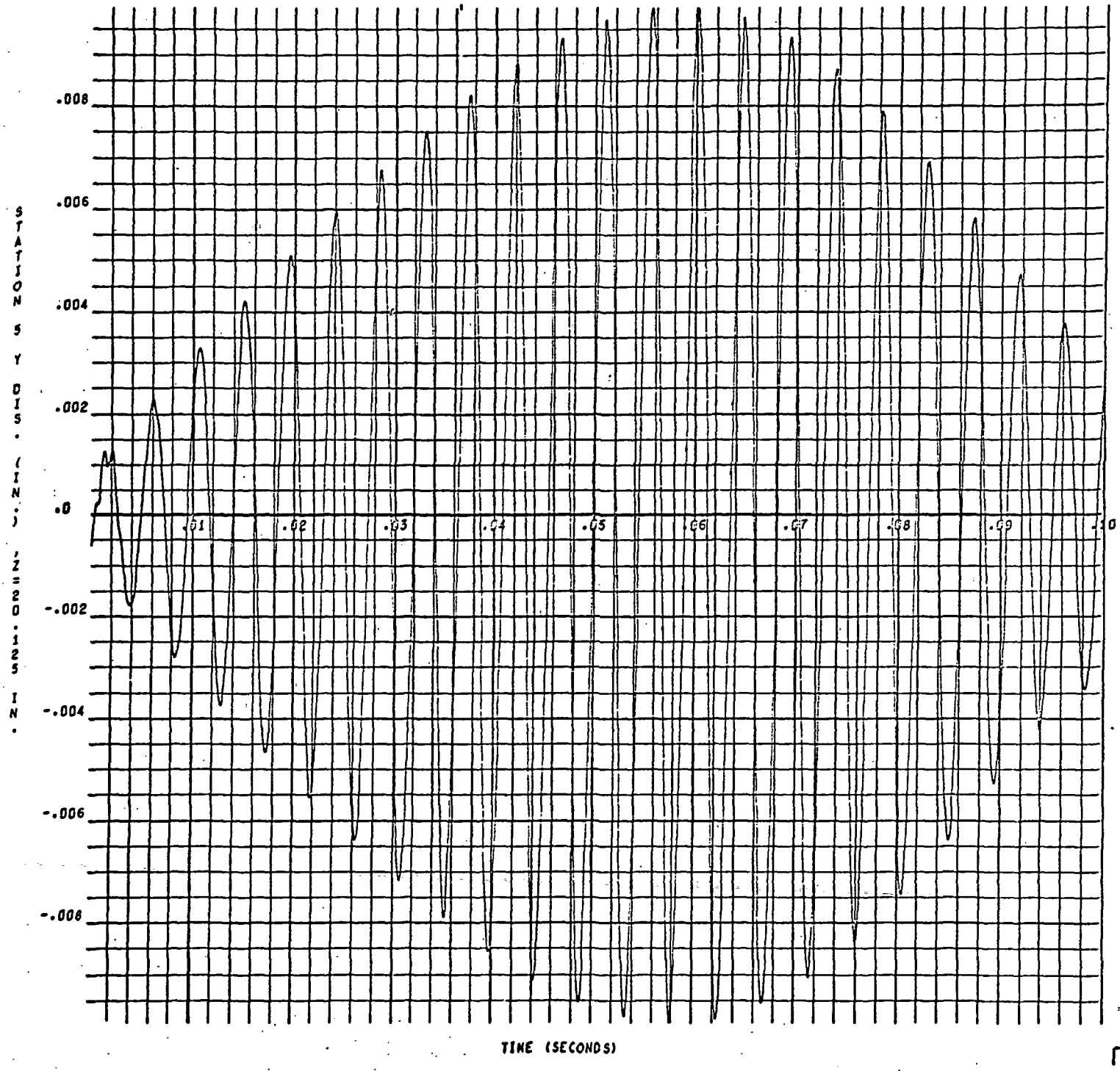

Figure 4(c) D. Childs

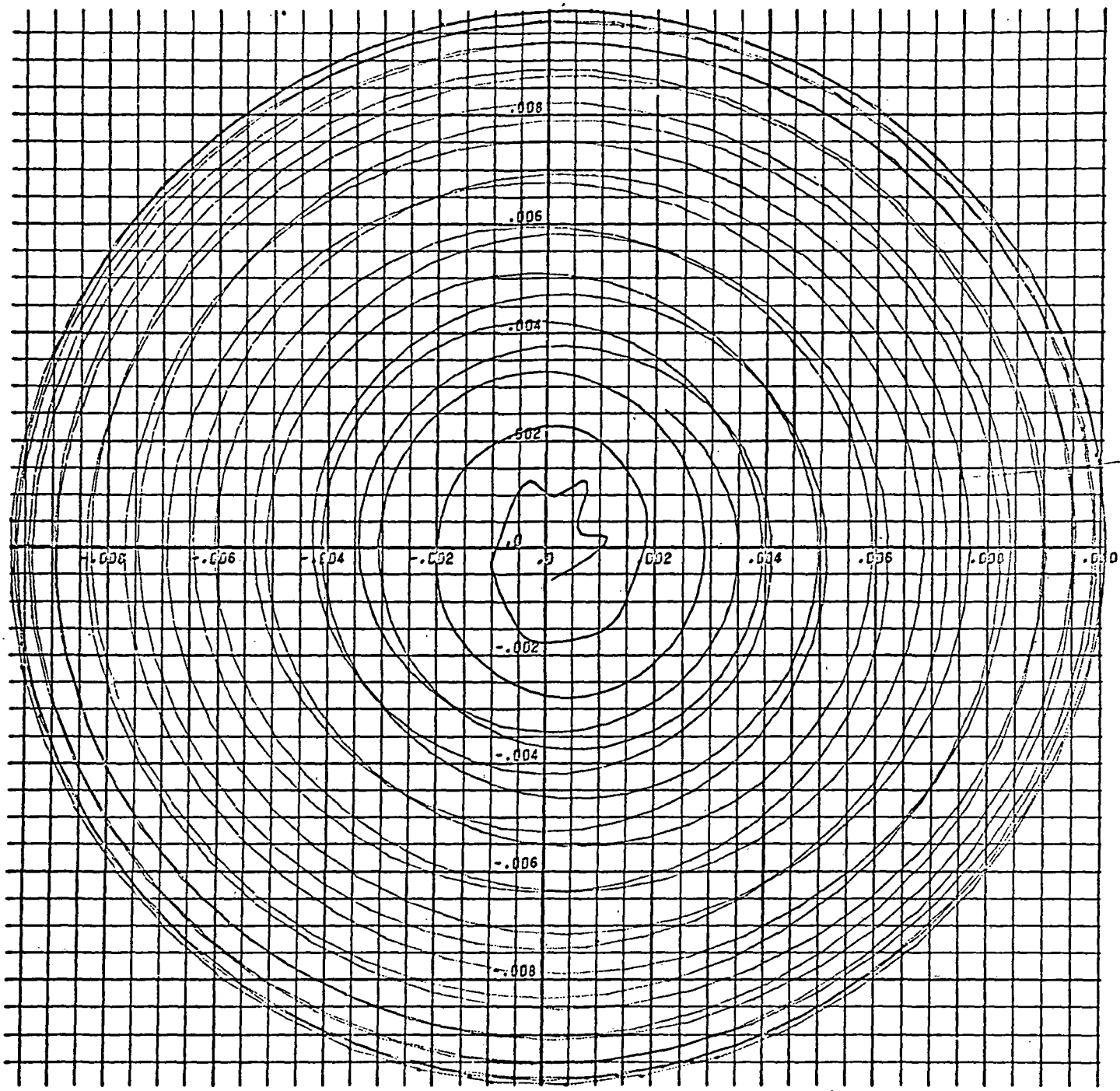

STATION 5 X DIS. (IN.) ,Z=20.125 IN.

Figure 4(d) D. Childs

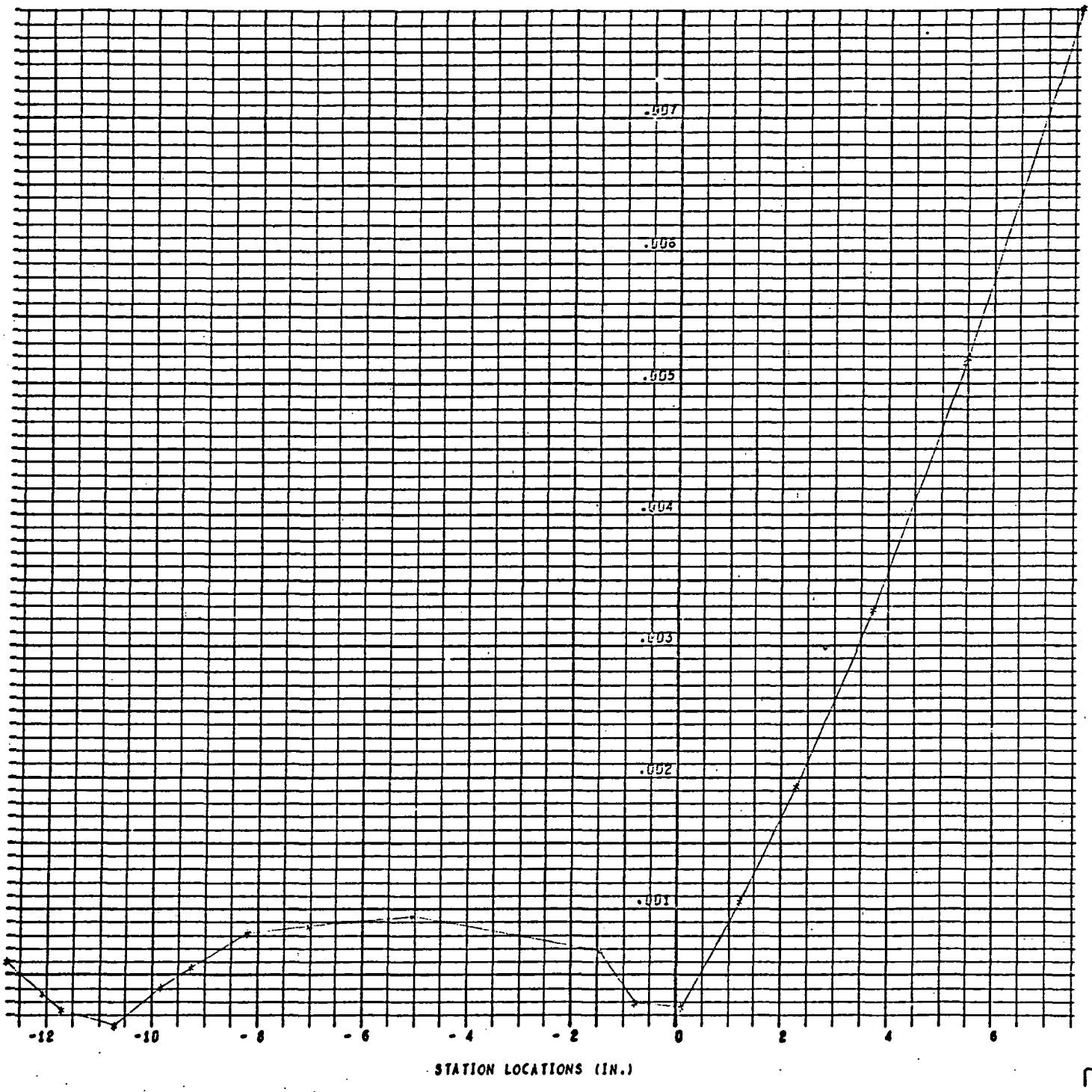

Figure 9(e) D. Childs

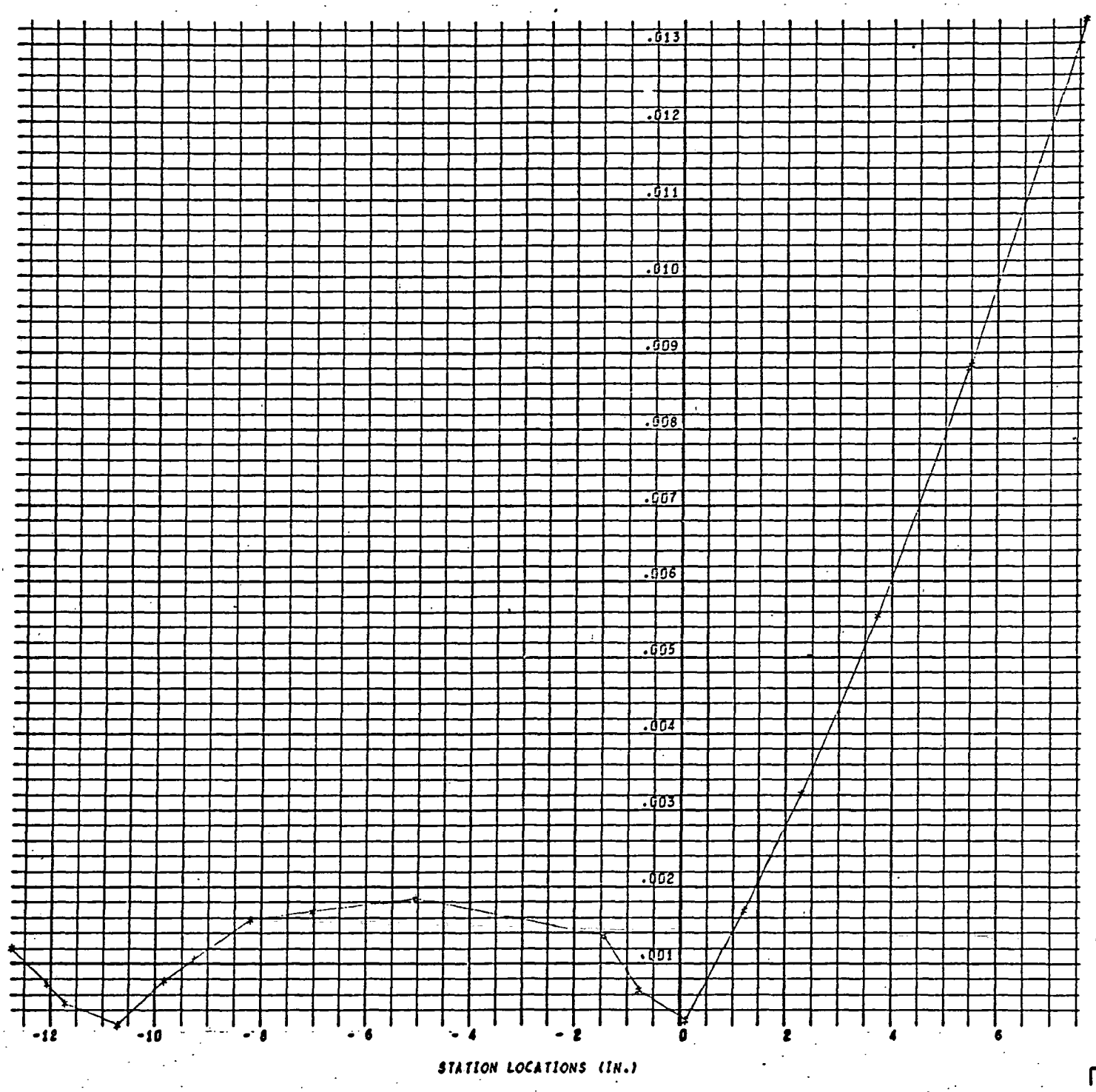

Figure 4(f) D. Childs

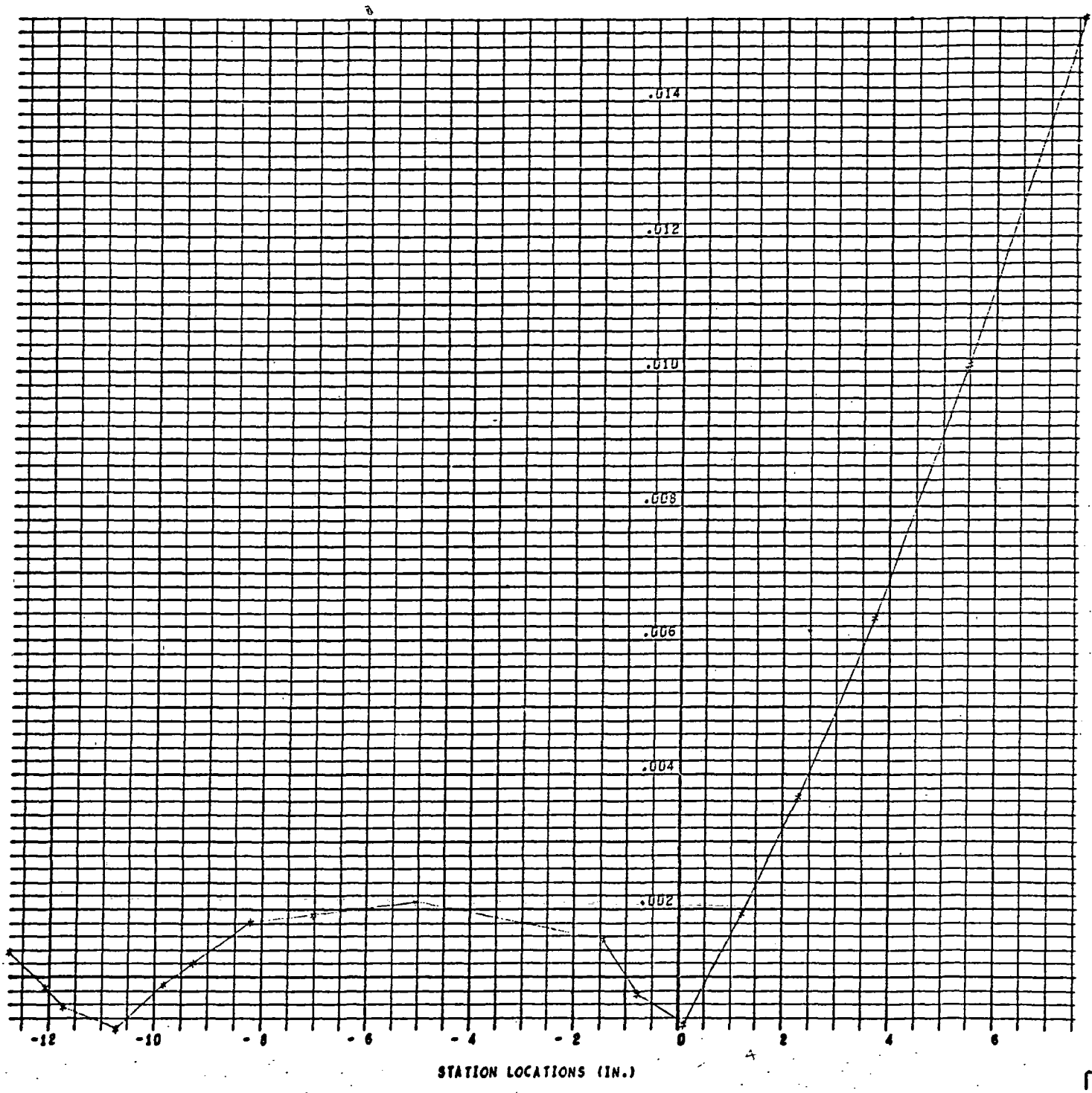

Figure 4(g) D. Childs

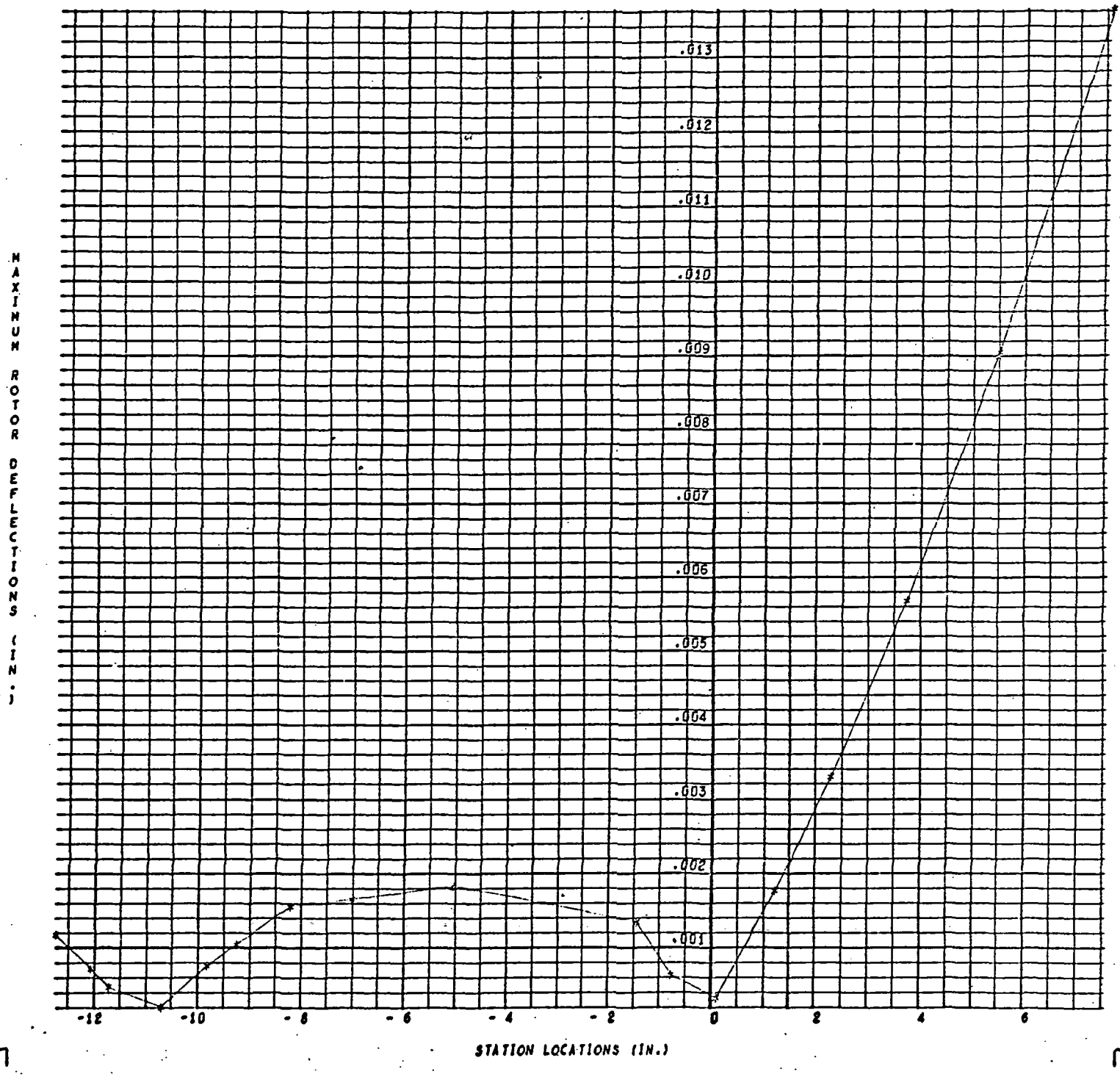

Figure 4(h) D. Childs

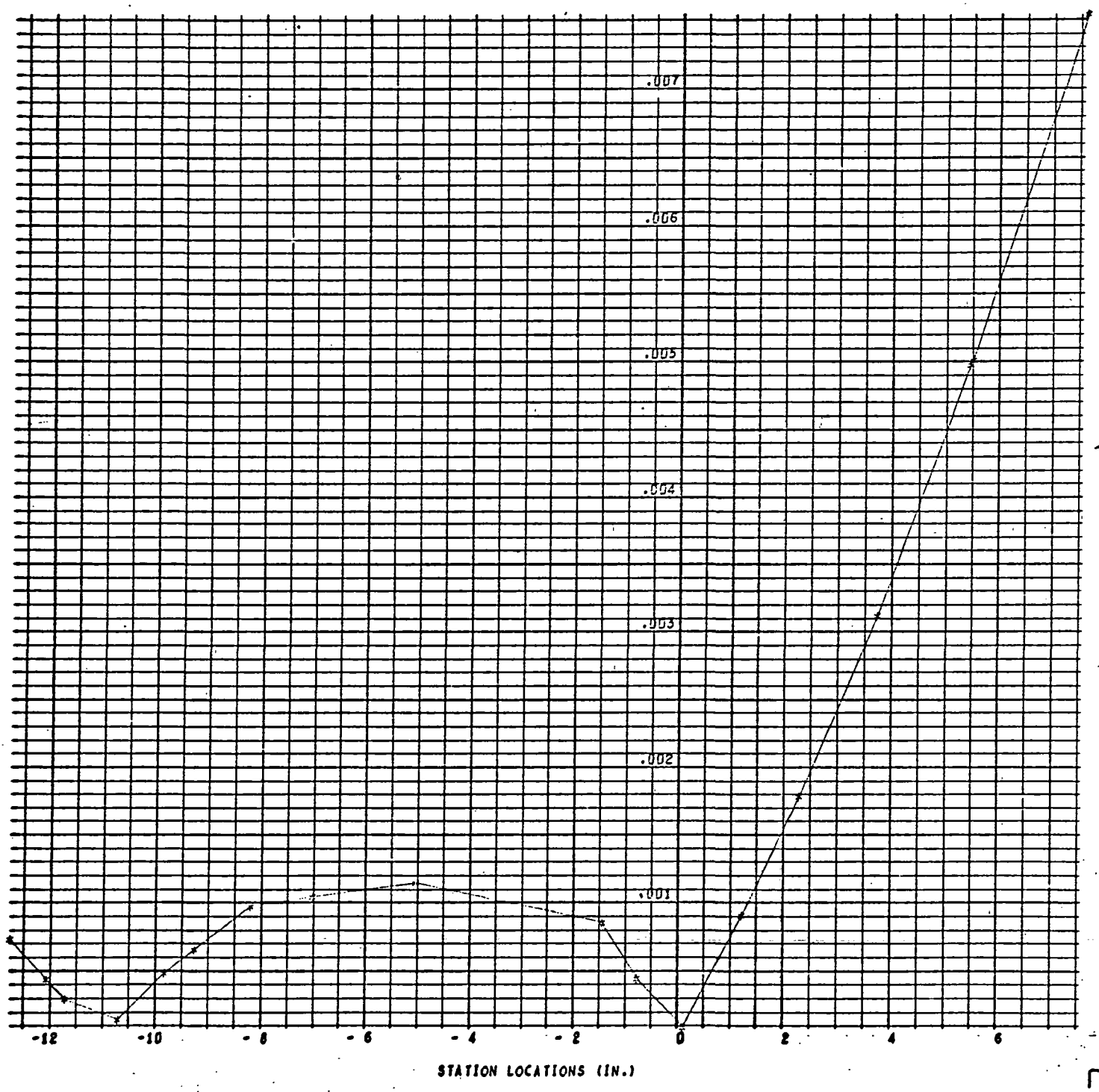

Figure 4(i) D. Childs

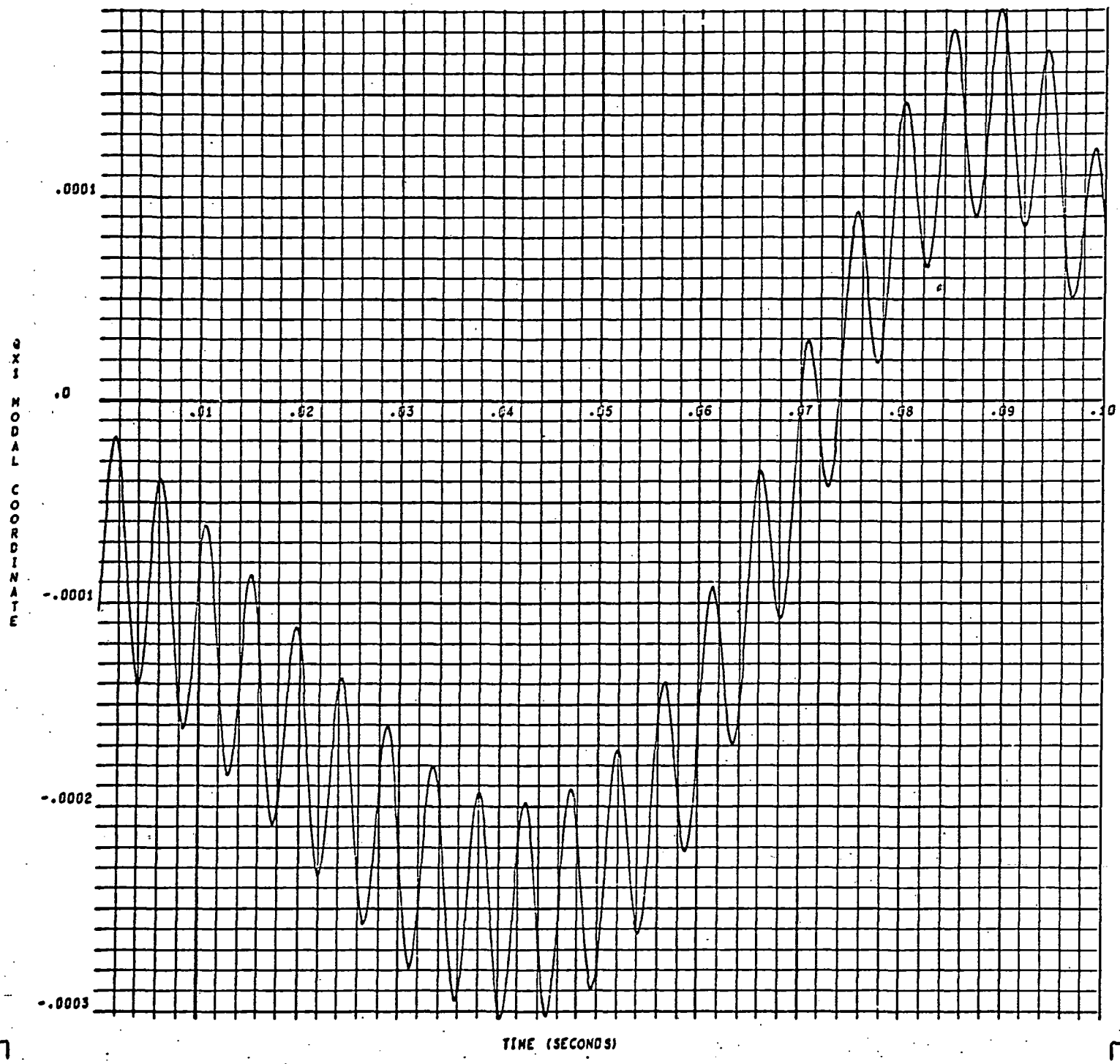

Figure 4(j) D. Childs

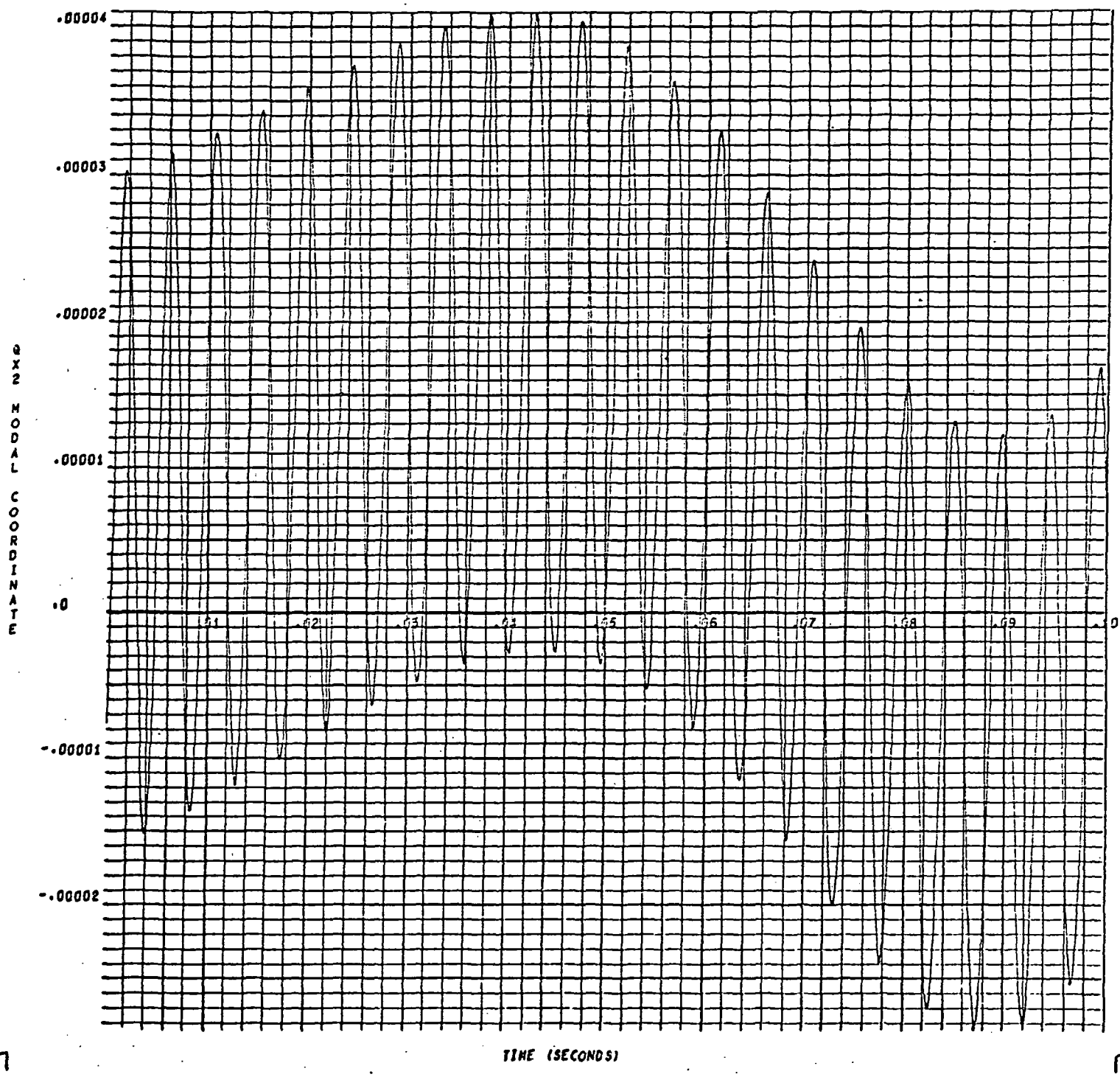

Figure 9(k) D. Childs

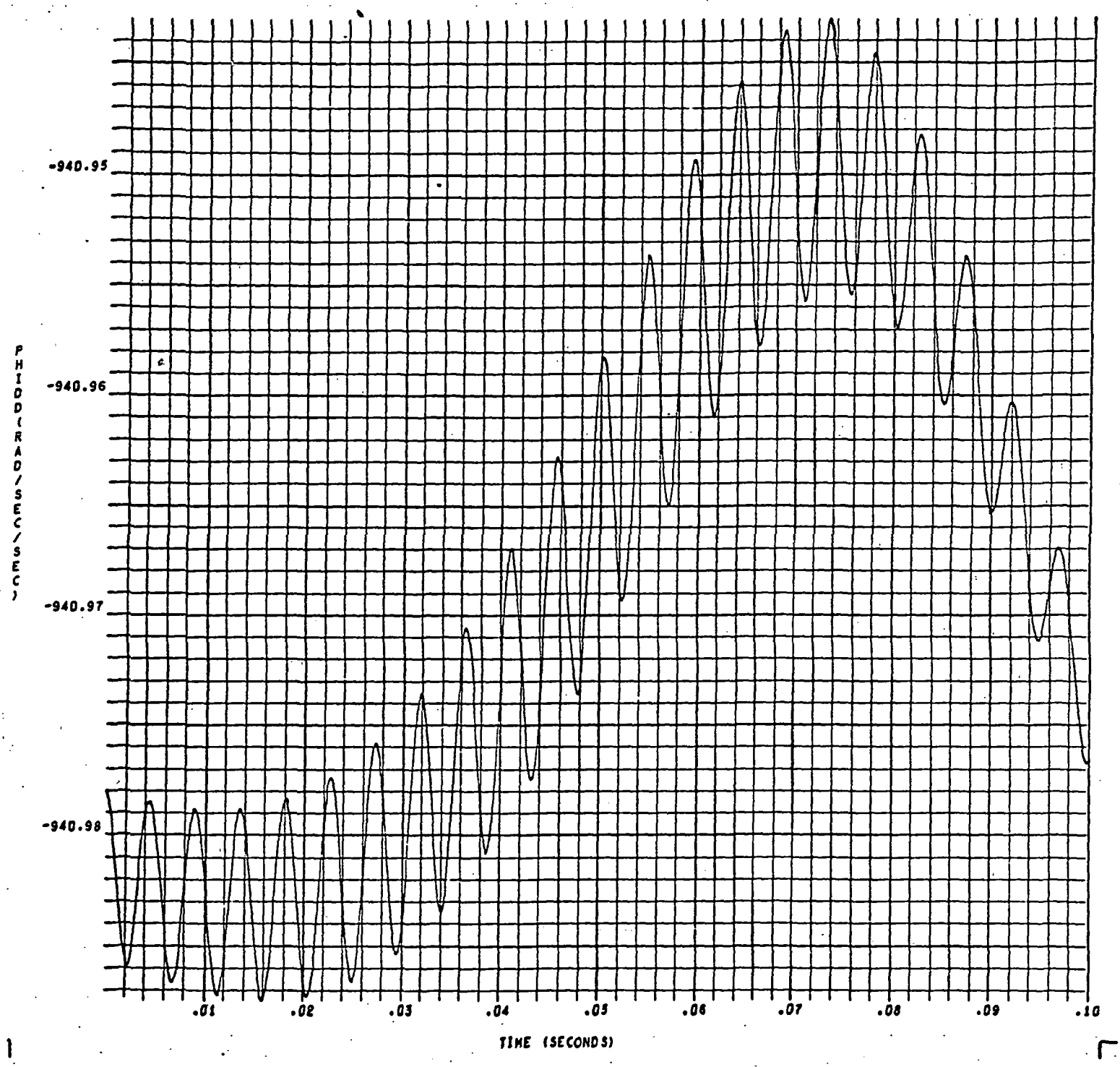

Figure 5 D. Childs

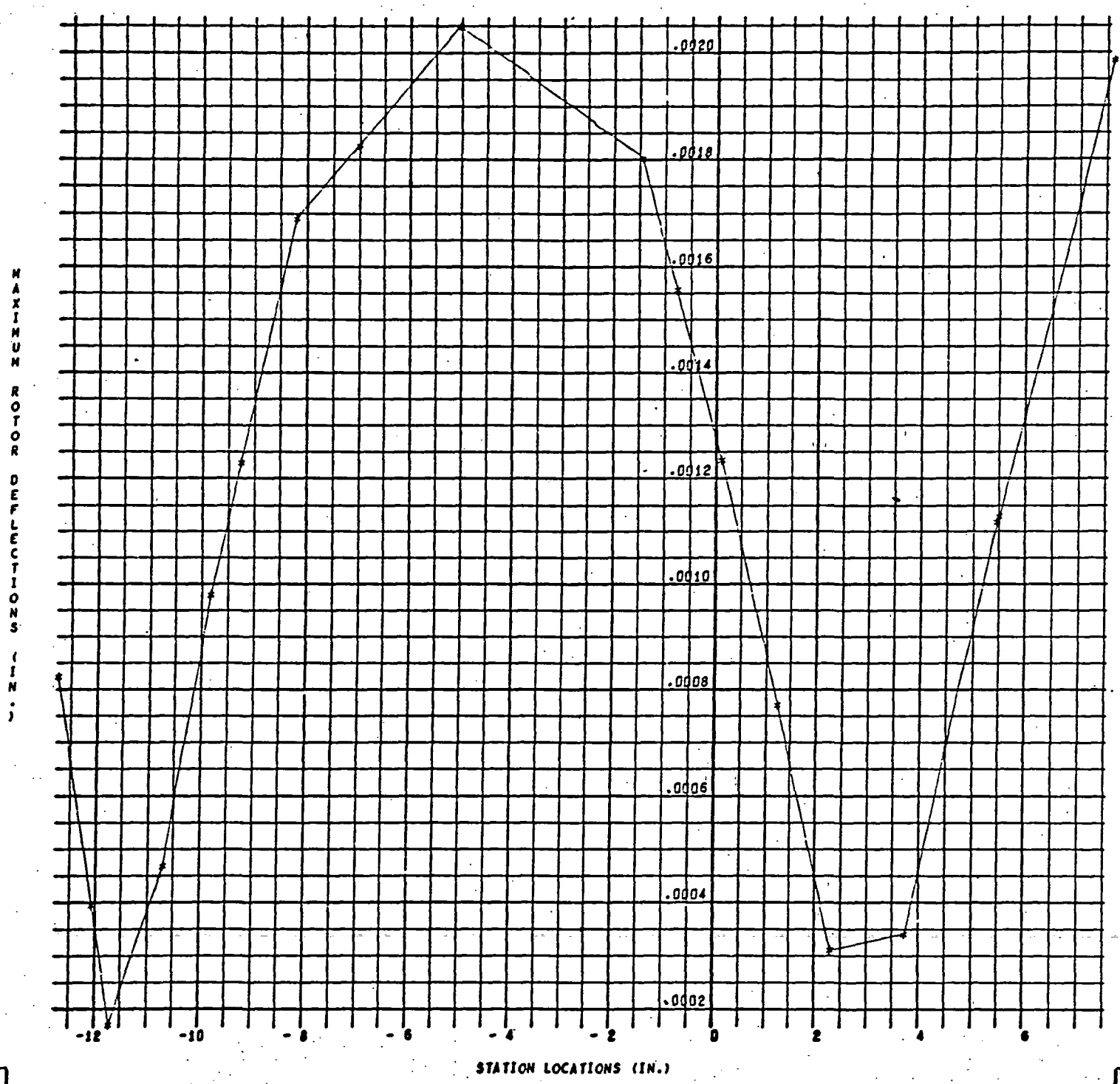

Fig. A.1. D.Childs

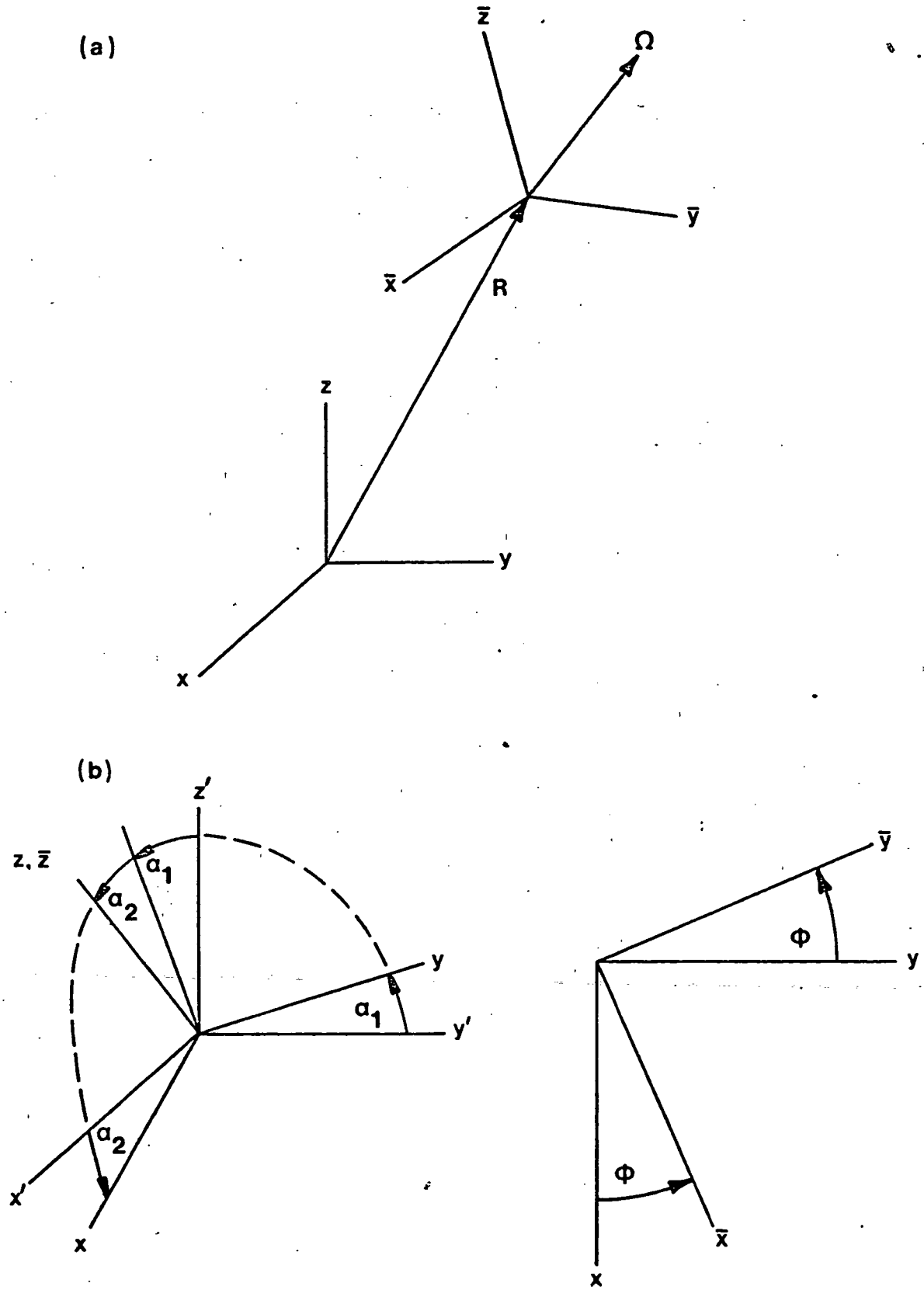
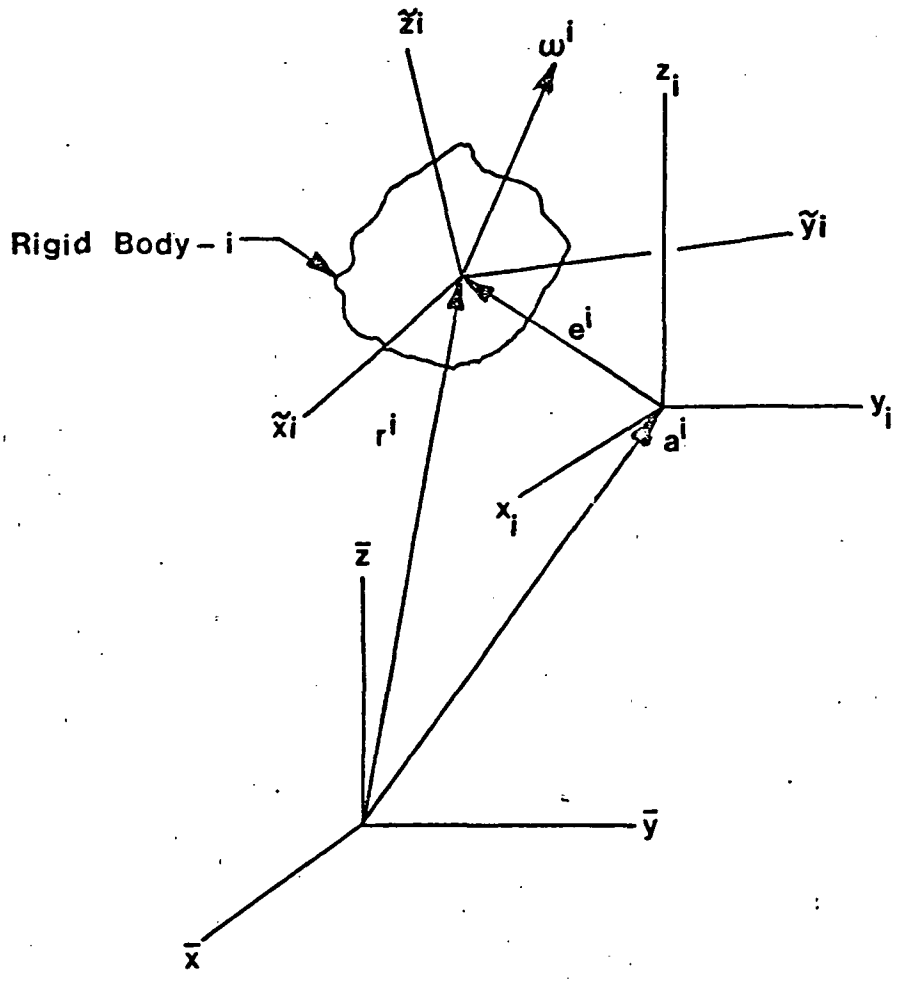
Fig. A.2. D.Childs